universität wien

MASTERARBEIT / MASTER'S THESIS

Titel der Masterarbeit / Title of the Master's Thesis

Plectin isoform 1c deficiency affects basic neuronal functions

verfasst von / submitted by

Katharina Bauer BSc

angestrebter akademischer Grad / in partial fulfilment of the requirements for the degree of

Master of Science (MSc)

Wien, 2020 / Vienna 2020

Studienkennzahl lt. Studienblatt / degree programme code as it appears on the student record sheet:	UA 066 834
Studienrichtung lt. Studienblatt / degree programme as it appears on the student record sheet:	Masterstudium Molekulare Biologie
Betreut von / Supervisor:	emer. o. Univ.Prof. Dr. Gerhard Wiche

Acknowledgments

I am most thankful to Univ. Prof. Dr. Gerhard Wiche for giving me the opportunity to work on this project and for his excellent support, supervision, scientific discussions and confidence in my work.

Many thanks to the lab and department members Eva Mihailovska, Lilli Winter, Maria Wiche-Castañón, Peter Fuchs, Irmgard Fischer, Fritz Propst, Petra Kalmann and Johanna Stranner for their help and support.
Special thanks go to Eva Mihailovska, who recommended me as master student candidate, supervised me in the first months of my thesis and tought me many techniques and methods, her friendly and humorful character was greatly appreciated. Special thanks go also to Lilli Winter for her straightforward help with scientific problem solving and proofreading of my thesis.

I thank my family for supporting me during my studies, always being patient and motivating and never questioning my chosen path of life.

“Don´t ever let someone tell you that you can´t do something. Not even me. You got a dream you gotta protect it.” “You want something go get it.”
(The Pursuit of Happiness)

I **STAND** upon my desk
to remind myself that
we must constantly
look at things
in a different way

Dead Poets Society

Summary

The 500 kDa polypeptide plectin is a versatile cytolinker that is crucial for intermediate filament networking including crosstalks with microtubules and the actin system. Its functional diversity is based on the alternative splicing of different first coding exons, resulting in a variety of isoforms that are differentially expressed in mammalian cells and tissues. This thesis is focused on plectin isoform P1c, which is mainly expressed in keratinocytes and neural cells. Previous studies had shown that in keratinocytes P1c acts as a destabilizer of microtubules and that its lack affects microtubule-dependent basic physiological functions such as cell division, glucose uptake, polarization and cell migration. The goal of my thesis was to investigate whether P1c played a similarly important role in neurons.

For this, I used P1c-deficient primary dorsal root ganglia neurons and hippocampal neurons to investigate the functional role of neural P1c. I showed that in the absence of P1c the organization and dynamic of the neurofilament network are disturbed, leading to alterations in neuritogenesis, such as outgrowth and branching of neurites. Monitoring DRG explants I could show that in the absence of P1c, DRG neurites become longer and grow faster. Additionally, through transient transfection and immunolabeling a rescue could be achieved leading to neurite lengths similar to those of WT cells. Branching experiments showed that in both DRG and hippocampal neurons lacking P1c, fewer branching points developed. Further, investigating the localization of neuronal P1c via double-immunolabeling I could demonstrate that P1c co-localizes with axonal microtubules in an isoform-specific way. Finally, using immunofluorescence microscopy and a high-speed centrifugation assay, I could show that the lack of P1c leads to increased association of tau protein with microtubule and increased levels of acetylated tubulin. These results point towards a crucial role in the organization and dynamic of microtubules.

Zusammenfassung

Das 500 kDa große Polypetid Plectin ist ein Zytolinker und spielt eine wichtige Rolle für die Interaktion des Intermediärfilament-Netzwerkes mit Mikrotubuli und dem Aktin-Zytoskelett. Basierend auf seiner Fähigkeit des alternativen Spleißens von unterschiedlichen ersten kodierenden Exons, entsteht eine Variation an Plectin-Insoformen, welche in den unterschiedlichsten Zellen und Geweben exprimiert werden. Diese Masterarbeit konzentriert sich auf die Untersuchung der Plectin-Isoform 1c (P1c), welche im hohen Maße in Keratinozyten und Nervenzellen exprimiert wird. Frühere Studien zeigten, dass P1c in Keratinozyten als Mikrotubuli-Stabilisator fungiert und dass durch die Abwesenheit von P1c grundlegende Mikrotubuli-abhängige physiologische Funktionen wie Zellteilung, Glukoseaufnahme, und Zellbewegung beeinträchtigt sind. Das Ziel meiner Studien war es zu untersuchen ob P1c eine ähnlich wichtige Rolle in neuronalen Zellen spielt und welche Auswirkungen dessen Abwesenheit hat.

Zur Untersuchung der funktionalen Rolle von P1c untersuchte ich Nervenzellen aus dem peripheren Nervensystem, sogenannte Dorsalganglien, und hippocampale Neuronen als Vertretter für das zentrale Nervensystem. In meiner Studie zeige ich, dass in Abwesenheit von P1c die Organisation und Dynamik des Neurofilament-Netzwerks beeinträchtigt ist und dies zu Änderungen in der Neurogenese führt. Die Untersuchung von DRG-Explantate zeigte unter anderem das in Abwesenheit von P1c Neurite schneller wachsen und insgesamt länger werden. Nach transienter Transfektion von P1c in P1c-KO DRG Neuronen erreichten deren Neurite wieder ähnliche Längen wie die der WT Neuronen. Die Quantifizierung neuronaler Verzweigungen („branching“) ergab, dass sowohl DRG als auch hippocampale Neuronen weniger Verzweigungen aufwiesen, wenn P1c abwesend war. Durch gleichzeitige Immunfärbung von P1c und Mikrotubuli konnte ich in dieser Studie weiter zeigen, dass P1c mit axonalen Mikrotubuli in einer Isoform-spezifischen Art und Weise interagiert. Im letzten Teil meiner Arbeit untersuchte ich welche Auswirkung das Fehlen von P1c auf die Dynamik und Organisation von Mikrotubuli hat. Durch Immunfärbungen intakter Neuronen und Zellfraktionierung mittels Hochgeschindigkeitszentrifugation konnte gezeigt

werden, dass in Abwesenheit von P1c mehr Tau an endogenes Mikrotubuli gebunden ist und erhöhte Werte für acetyliertes Tubulin vorhanden sind. Beide Resultate sind Hinweis darauf, dass P1c wichtig für die Organisation und Dynamik von Mikrotubuli ist.

Introduction

The research focus in this master thesis is the investigation of elementary functions of plectin 1c (P1c) in neuronal cells. Therefore, the first part of the introduction addresses the nervous system and the two main neuronal cell types used in my experiments: hippocampal neurons of the central nervous system (CNS) and dorsal root ganglion neurons (DRG) of the peripheral nervous system (PNS). The following chapters introduce the three network systems that form the cytoskeleton of neurons and provide information about the cytoskeleton crosslinker plectin, in particular its isoform P1c. The final chapter in the introduction gives a short overview about plectinopathies, diseases caused by plectin deficiencies.

The nervous system

The two parts of the nervous system, the CNS and the PNS, are formed by the brain, the spinal cord, the sensory organs and all the nerves that have a connecting function between them. These various parts are responsible for the transmission of external signals to the brain and the response to signals within the organism. The CNS is known as the control center, where information is evaluated, and conclusions are made. The PNS consists of the sensory nerves and organs that screen the inside and outside conditions of the body and transmit information to the CNS, whereas the efferent nerves carry signals from the CNS to the glands, muscles and organs. Neurons and neuroglia cells are the two main classes of cells forming the nervous system. Glial cells can be subdivided into four major groups microglia, oligodendrocytes, astrocytes and the NG2-glia progenitors. These cells play an important role in the maintenance of the blood-brain-barrier, the secretion and absorption of neurotransmitter and the migration of neurons. Neuronal cells therefore can be subdivided into three main classes: afferent, efferent, and interneurons. Afferent neurons also known as sensory neurons transmit sensory signals from the body periphery to the CNS. Efferent neurons and motor neurons transmit signals from the CNS to so called effectors in the body, such as glands and muscles. Interneurons form complex networks within the CNS to react to incoming signals from the afferent neurons and to direct

the functions of the whole body through efferent neurons. All types of neurons have a stereotypic structure shown in Fig. 1, with a soma (cell body), containing the nucleus, many short and branched dendrites to receive signals, and one long axon with a presynaptic ending (axon terminals) to transmit information to neighboring cells. Along the axon, microglia called astrocytes and oligodendrocytes are wrapping around to support neurons and synapses.

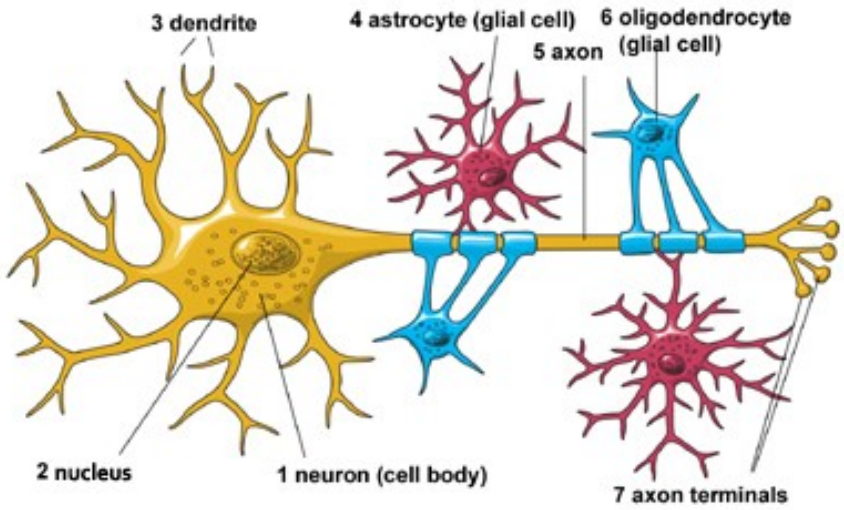

Figure 1. The architecture of neurons

The neuron (yellow) consists of three parts: the cell body (1) with the nucleus (2) extending dendrites (3), and the axon (5). At the end of the axon, terminals (7) also called synapse, for transmission of information, are located. The axon itself is protected by two types of glia cells: astrocytes (4, red) and oligodendrocytes (6, blue). *Image and legend from National Institute of Neurological Disorders and Stroke; Brain Basics: The Life and Death of a Neuron*

In the following two subchapters I will give short overviews over the CNS and the PNS, with focus on hippocampal and DRG neurons, the two types of neurons I was studying in this thesis.

The central nervous system

The CNS is the processing center of the nervous system and the two main organs are the brain and the spinal cord. The brain, located in the cranial cavity and protected through the skull and the brain-blood barrier, processes and interprets sensory information from the spinal cord and sends information to the

PNS as response. The spinal cord is located in the spinal cavity and consist of 31 nerves protected by the vertebrae.

The **hippocampus** (lat. word for seahorse) is an essential structure of the limbic system in the brain and has important functions in producing, controlling and recalling information into and from the long-term memory. Hippocampi are located in both hemispheres of the brain, at the bottom of the lateral ventricle from the temporal lobe (Fig. 2).

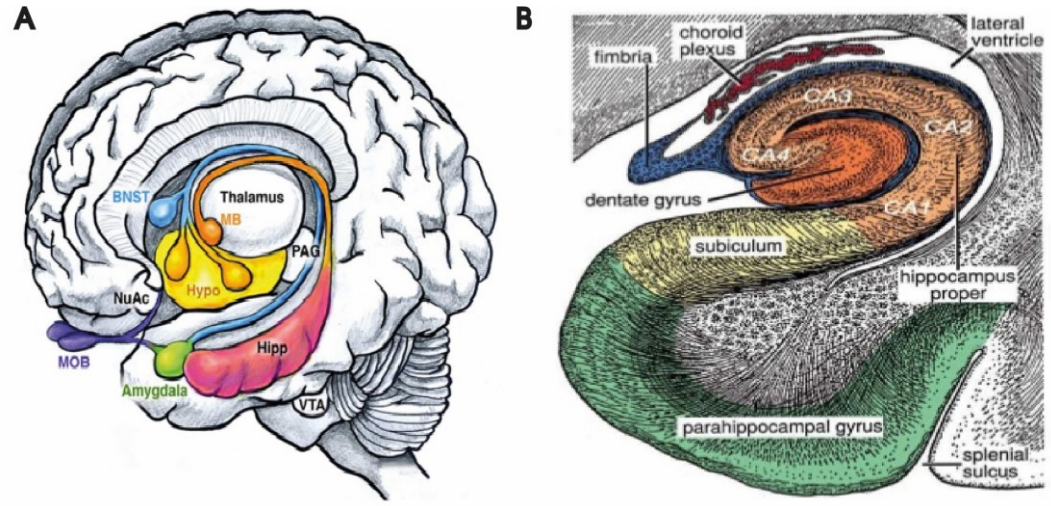

Figure 2. Cross section of the limbic system and schematic drawing of the hippocampal structure

(A) Human brain showing the amygdala (green), bed nucleus of stria terminalis (BNST, blue), hypothalamus (yellow), and hippocampus (pink). The hippocampus (pink) attaches to the mamillary bodies (orange) through the fimbria-fornix. Olfactory inputs are received by the olfactory bulbs (MOB, purple). Other structures include the nucleus accumbens (NuAc), ventral tegmental area (VTA), and the periaqueductal gray (PAG) (Sokolowski and Corbin 2012). (B) The hippocampal formation consists of the dentate gyrus (dark orange), hippocampus proper (pale orange), and subiculum (yellow). The latter is continuous with entorhinal cortex covering the parahippocampal gyrus (green). The hippocampus proper (cornu ammonis) may be divided into four regions (CA1…CA4). Output axons (blue) from the hippocampal formation run superficially in the alveus and then in the fimbria. The subiculum conveys reciprocal connections between the hippocampus and entorhinal cortex. The hippocampus forms a partial wall of the lateral ventricle, which contains a choroid plexus (Modified from *Ranson, S.W. and Clark S.L. 1959 Anatomy of the Nervous System, 10th ed. Philadelphia, W. B. Saunders Co*).

Fig. 2A shows the architecture of the limbic system, consisting of a collection of different brain structures from many brain areas. It is located in the

midbrain behind the frontal cortex and beneath the corpus callosum, and it surrounds the thalamus in both hemispheres. Including not only the hippocampus but other structures such as the olfactory bulbs (important for the sense of smelling), mammillary body (involved in memory processing), the septum pellucidum and the fornix (having connective functions), and many more brain structures, the limbic system is functionally important for emotion, behavior and long term memory processing. On the occipital side, the lower back part, the hippocampus ends in the fornix (a bundle of nerve fibers that acts as an output tract) and can so interact with other parts of the brain. Further on it gains information about the body´s awareness from the entorhinal cortex (not shown). The hippocampus itself is divided into three structural parts. One is the dentate gyrus (Fig. 2B), considered as the “entrance”. Any information from the sensory organs arrives here and the interneurons inhibit then the intensity of the signals. The next sector, divided into 4 areas CA1-CA4, is the cornu ammonis, which is important for selecting the information (Fig. 2B). The last instance during information processing, the subiculum forwards the selected information to the parahippocampal gyrus. Between all these hippocampal parts many neuronal networks exist to ensure flawless communication. Dysfunctions or loss of both hippocampus regions have a dramatic effect on the memory, patients will still be able to recall information, but newly gained knowledge cannot be memorized. The information processing from short- to long-term memory is one of the most important functions of the hippocampus. It generates new information and coordinates already acquired knowledge. Consequently, humans will be able to orientate them easily in a familiar area but will need more time in unknown settings.

The peripheral nervous system

The PNS is the connection between the CNS and the periphery. Sensory signals are sent to the spinal cord and motor output is created as response. Two classes of neurons belong to the PNS: the autonomic and the sensory nerves. The autonomic nervous system regulates breathing and digestion; while the somatic nervous system is important among others for body reflexes.

As part of the PNS, DRGs are sensory neurons that transmit messages from the periphery to the spinal cord. DRGs form clumps of nerve tissue located

along the dorsal roots of cervical, thoracic, lumbar and sacral spinal nerves near the entry of the spinal cord. As shown in Fig. 3, DRGs form pseudo-unipolar structures where their cell bodies are located inside the dorsal root ganglion and the cell protuberance divides then into a long dendrite, known as somatic- or visceral- sensory neuron that extends to the periphery and into the axon (dorsal root) which ends in the posterior horn of the spinal cord. Interneurons in the posterior horn receive input from the somatic sensory (SS) and the visceral sensory (VS) neurons, while the anterior horn receives signals from visceral motor (VM) and somatic motor (SM) neurons.

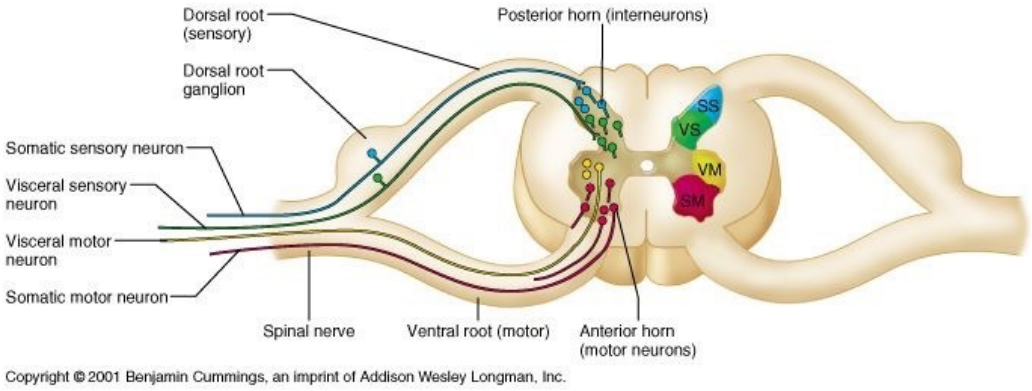

Figure 3. Anatomic location of DRG neurons

DRGs are located along the spinal cord. A transversal plane section on the spinal cord reveals the location and structure of the neurons in details. The DRG harbors the neuron cell body. The posterior horn contains the inlets of the somatic sensory neurons (blue), the visceral sensory neurons (green), whereas the anterior horn harbors the sensory motor neurons (red) and the visceral motor neuron (yellow). Image: Copyright © 2004 Pearson Education, Inc., publishing as Benjamin Cummings Human Anatomy & Physiology, Sixth Edition Elaine N. Marieb PowerPoint ® Lecture.

Injuries or deficiencies affecting DRG neurons often lead to diseases of the PNS, so called peripheral neuropathies. Peripheral neuropathy is a common definition including hereditary neuropathies (e.g. Charcot-Marie-Tooth disease), motor or sensor neuropathies, polyneuropathies, ganglionopathies and many more. In most cases the cause for the development of the neuropathy has not been determined, but most patients have the same or similar symptoms (weakness affecting feet, legs, hands and torso, feeling numbness in face and

tongue). Furthermore, abnormal response to temperature, vibration, touch and pain, and abnormal reflexes could be identified as physical characteristics in patients with peripheral neuropathy. Peripheral neuropathies can manifest as a disorder of the axon and/or the myelin within nerve fibers (Podgorny and Toth 2014; Sghirlanzoni, Pareyson, and Lauria 2005; England and Asbury 2004).

Development and growth of neurons: growth cone and branching

Neurons form through a process called neurogenesis. They arise from the embryonic neural tube that contains progenitor cells. After various cell divisions and differentiations, the newly synthesized neurons migrate to their final locations, where they lose their ability to multiply, differentiate, and extend axons. For migration and neurite outgrowth, neurons need external signals from the surrounding that are detected by the growth cone of the neuron.

Neuronal growth cone

Growth cones are highly dynamic and motile structures at the leading edge of neuronal axons. They are guiding the axon to specific targets by responding to external cues that affect signaling pathways involved in the regulation of their cytoskeleton networks, in particular filamentous (F)-actin and microtubules (MTs). Changes in the organization and dynamics of these networks lead to alterations of growth cone shape and locomotion, thereby determining the direction of axonal outgrowth. Typically, growth cones are fan-shaped structures at the distal tip of the axon, that vary their sizes and shape through extension and retraction of membrane protrusions (reviewed in Dent and Gertler 2003). Depending on their size and shape, protrusions are referred to as filopodia (long and narrow) or lammellipodia (short and wide). This very dynamic peripheral region of growth cones transits into the more stable central region, which is less dynamic but still exhibits molecular motion through shuttling of organelles and vesicles. The central region boarders directly onto the cylindrical shaft of the axon. The growth cone undergoes constant dynamic changes in its structure driven by specific cytoskeletal changes (Dent, Gupton, and Gertler 2011). During axon outgrowth, the growth cone shows three different structural stages: extended protrusions, engorgement, and consolidation. The first stage, is characterized by membrane

extensions through F-actin polymerization, the second by MT guided delivery of membranous organelles and vesicles to the peripheral region, and the third, by growth cone contraction and stabilization onto a cylindrical axon shaft (Goldberg and Burmeister 1986).

Neuronal branching

Branching is the ability of neurons to extend multiple dendritic and axonal branches and form terminal arbors to communicate to each other. During development of the nervous system the regulation of the axonal branching must be tightly controlled to ensure the optimal progress of neurite outgrowth, synaptic interactions, and neuron maturation. It was shown by Craig and Banker (1994), that neuronal polarity is a requirement for the proper working of branching mechanisms. Typically, all neurons have a long primary axon with periodic collateral or distal branches. Further on, they have multiple primary short axons around their cell body. Usually axonal branches can form through bifurcation of the growth cone or through formation of interstitial branches along the axon shaft. Different research groups have shown that cytoskeleton network dynamics are essential for branching. In particular, interstitial branching requires destabilized MTs (Jeanneteau et al. 2010). Accordingly, overexpression of MT severing proteins (e.g. spastin or katanin which break long MTs into shorter pieces) leads to newly forming branches (Yu et al. 2008, Qiang et al. 2010). Furthermore, it was observed that the plus end tips of MTs interact with the actin cytoskeleton network to form new branches (Kornack and Giger 2005).

The neuronal cytoskeleton

Cells need a well-organized cytoskeleton network system to fulfil different functions, including cell growth, migration, intracellular traffic of organelles, transport of proteins, interactions with the environment, and proper cell shape. The cytoskeleton stabilizes the cell mechanically, determines its shape and provides the platform for internal signaling. The cytoskeleton is an intracellular filamentous system, consisting of three different types of filaments: *actin filaments, MTs and intermediate filaments*. Each filament is composed of small protein subunits and interacts with numerous accessory proteins that regulate

their assembly and disassembly, convert ATP hydrolysis into mechanical force, and control the movement along the filaments. Through their ability to rapidly undergo structural reorganization, through assembly and disassembly of subunits at their ends and at different locations, the filaments form dynamic and stable structures, provide large scale cellular polarity, and are responsible for cellular organization. Providing stable and large-scale structures is especially important for the cellular organization of mature neurons. Furthermore, during development and migration, the growth cone at the leading end of the axon guides the neuron to its synaptic target. While the axon is a long membrane-bound extension containing MTs and neurofilaments (NFs) as cytoskeletal elements, the growth cone and its filopodial extensions contain mostly actin filaments.

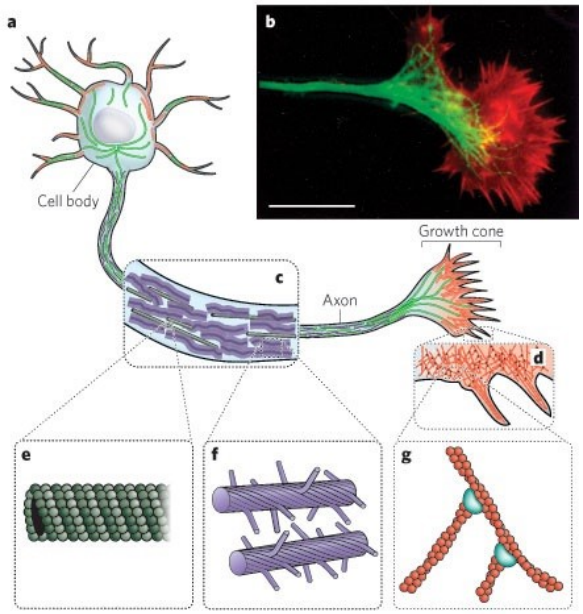

Figure 4. The cytoskeleton of neurons

(a) Neurons have a cell body with many short dendrites and one long axon with a growth cone. (b) Immunofluorescence microscopy of the axon and growth cone, using antibodies to MTs (green) and actin (red). Scale bar, 20 μm. Note, MTs emanate from the axon into the growth cone while the actin filament network is concentrated in the peripheral area of the growth cone forming sheet-like structures and filopodial protrusions. (c) The neuronal axon contains MTs and NFs, which transport vesicles, lipids, proteins and other cell parts from the cell body to the growth cones. (d) The growth cone contains different actin network systems: a dendritic actin network in the lamellipodia and tight parallel bundles in the filopodium. (e) MTs represent hollow tubes, formed by 13 protofilaments. (f) NFs have numerous flexible side arms which regulate the radius of the axon. (g) Actin filaments have many different networks formed by many complexes; e.g. Arp2/3 complex (blue). Image from Nature; (Fletcher and Mullins 2010).

Actin filaments

Actin filaments (or microfilaments) are built up of ~43 kDa globular (G)-actin monomers (carrying tightly associated ATP or ADP molecules) that first assemble into long protofilaments, two of which then twist around each other to form a long filamentous polymer (F-actin) with a diameter of ~7 nm. Microfilaments have a thin and flexible structure with a helical repeat every 37 nm and at least 13 actin subunits between every cross-over-point. Three versions of actin monomers are known, namely α, β and γ actin, differing slightly in their amino acid sequences. Actin subunits assemble head to tail and form polarized structures with a plus (barbed) and a minus (pointed) end. Actin molecules at the barbed end are bound to ATP, which favors the incorporation of more actin-ATP complexes, leading to filament assembly, and thus growth. The actin subunits at the minus end are bound to ADP, which favors filament disassembly and shrinkage. This situation leads to the phenomenon of treadmilling, where there is a consistent flow of actin subunits from the plus to the minus end of the filament. Various cell types such as neurons use the dynamic properties of actin filaments to their advantage to orientate and elongate the plus end towards the leading edge of the cell, thereby, pushing the plasma-membrane forward. Actin filaments in mammalian cells are arranged in several network forms, crosslinked and bundled by accessory proteins. Neurons favor dendritic filament structures or tight parallel bundles. Dendritic networks are nucleated by an Arp2/3 complex that attaches the pointed filament end to the side of other filaments present in lamellipodia. Whereas in filopodia one finds tightly packed bundles consisting of crosslinked parallel filaments (Svitkina and Borisy 1999).

Microtubules

Another type of cytoskeletal filaments found in all eukaryotic cells are the MTs. They consist of α and β tubulin heterodimers assembled in head-to-tail formation. Alpha and β tubulin subunits both have a molecular mass of about 55 kDa and both harbor a nucleotide binding site. While the GTP bound to α tubulin will never undergo hydrolysis, β tubulin can bind either GTP or GDP. As shown in Fig. 5A, MTs are composed of α and β tubulin heterodimers forming

protofilaments with GTP bound α and β tubulin at the plus end and GDP bound α and β tubulin at the minus end.

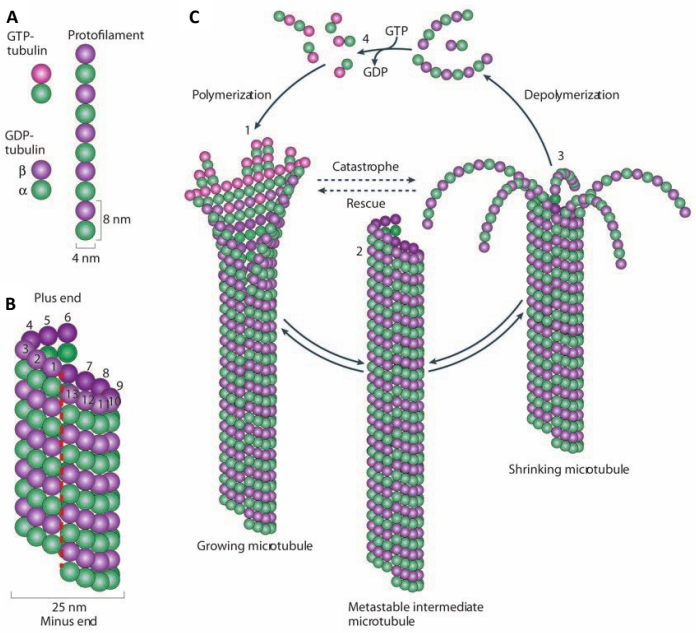

Figure 5. Microtubule structure and dynamic instability

Microtubule structure and dynamic instability. (A) Protofilament structure. (B) Microtubule structure. (C) Illustration of dynamic instability. (1) growing microtubule, (2) metastable intermediate microtubule, (3) shrinking microtubule, (4) GTP hydrolysis. Reprinted from (Akhmanova and Steinmetz 2008), with permission from Nature Publishing Group, license No. 3134720753071, Apr 23, 2013.

Thirteen protofilaments form a hollow cylindrical structure with a diameter of about 25 nm (Fig. 5B). The bottom part of the α tubulin monomer interacts with the top part of the β tubulin monomer via longitudinal contacts. Furthermore, each one of the α and β monomers makes lateral contacts with their counterparts in neighboring protofilaments. Consequently, all protofilaments show the same orientation and are aligning in parallel, leading to the formation of a polarized cylinder. MTs are very flexible and dynamic structures showing the phenomenon of dynamic instability. Metastable intermediate MTs can shrink and grow depending on the hydrolysis rate of its bound GTP (Fig. 5C). Usually filaments are protected by GTP-caps, produced by the addition of GTP-bound subunits to the plus end. If nucleotide hydrolysis proceeds faster than the addition of subunits, the filaments lose their protective caps and undergo rapid shrinkage, called

catastrophe. During the state of catastrophe, GTP-bound subunits are still added to filaments, leading to new protective GTP-cap and a rapid growth of the filaments (rescue). The minus end of the MT is unstable and shrinks unless it is stabilized by capping proteins. In neurons, MTs are usually extremely stable and have a long life span. Moreover, axonal MTs serve as a scaffold for the transport of organelles and structural components of the neurites, and thus are indispensable for neurite elongation. In addition, by interacting with actin microfilaments in developing neurons, MTs play an important role in axon guidance by regulating growth cone morphology and motility (Dent, Gupton, and Gertler 2011).

Alpha and β tubulin subunits can be modified by multiple posttranslational modifications (PTM) to form a “tubulin code”, which can be read by some factors that interact with MTs (Verhey and Gaertig 2007). PTMs are usually highly dynamic and often reversible processes that can alter the functional properties of proteins. Modifications, such as methylation, phosphorylation, ubiquitination, acetylation and many others, take place on amino acid residues by addition of chemical groups or other peptides and proteins. As major cytoskeletal components and substrates for PTMs, tubulin and MTs play an essential role in cell development, growth, motility, and intracellular trafficking. Acetylation is of special interest for this thesis, as it is one of the main modifications taking place on the tubulin heterodimers and thus is playing an essential role in neuronal development (Westermann and Weber 2003).

Acetylation was first reported in the 1980s by L’Hernault and Rosenbaum (1985), who found that acetylation of the epsilon amino group of lysine at position 40 of α tubulin occurs in assembled MTs. Acetylation of MTs is considered to be a marker for the MTs age, as acetylated MTs are softer and more resistant against mechanical stress and turnovers (Portran et al. 2017). Although, under depolymerizing conditions (nocodazole or colchicine treatment) acetylated MTs are more stable than non-acetylated ones, it seems that acetylation and stabilization are independent from each other. The acetylation of K 40 protects MTs from depolymerization by making them softer and thus resistant to damage (Piperno, LeDizet, and Chang 1987; Wilson and Forer 1997; Reviewed by Janke and Montagnac 2017). Acetylation does not affect polymerization/ depolymerization of tubulin (Perdiz et al. 2011) and can occur on very dynamic

MTs. In mature neurons acetylated MTs are primarily found in proximal regions of the axon and are less abundant in the cell body, the growth cone, and dendrites. In young neurons, undergoing neurite outgrowth, increased levels of acetylated tubulin could be found in the proximal region of neurites and in the cell body (Fukushima et al. 2009; Perdiz et al. 2011; Witte, Neukirchen, and Bradke 2008). Creppe considered that MT acetylation could be relevant for migration, differentiation and synaptic targeting of neurons (Creppe et al. 2009). As another aspect, it was suggested that MT acetylation together with other modifications could have an influence on the transport and binding of microtubule associated proteins (MAPs) (Hammond et al. 2010).

Three classes of proteins interact with MTs: i) MT associated proteins (MAPs) which by binding to tubulin stabilize and promote MT assembly; ii) motor proteins, which use the energy of ATP hydrolysis to generate movement along MTs (kinesin and dynein); and iii) a group of proteins that associates with MTs including kinases and glycolytic enzymes e.g. GAPDH (Mandelkow and Mandelkow 1995).

MAPs, the major study object of my work, can be split into two categories according to their binding preference; either to specific sites or all along the MT length. The best categorized MAPs are MAP1a, MAP1b, MAP2, MAP4 and tau. MAP1a and b are high molecular weight proteins that associated with small polypeptides bind to and stabilize MTs. MAP1b is first detected during neuritogenesis and is required for the development of the nervous system. It is expressed at high levels in developing neurons but at much lower levels in the adult CNS. MAP1a is present in adult neurons but is expressed at a 10-fold lower level in developing neurons. MAP4 is a non-neuronal MAP, that shows molecular domains with MAP2 and tau and as like them promotes MT assembly. MAP2 and tau belong to the same family of MAPs. They share similar MT-binding domains but differ at the cellular level by being targeted to different cell compartments of the neuron. While MAP2 is mainly found on dendrites, tau is localized in axons.

MAP2, MAP4 and tau have alternative splice forms, sharing a conserved C-terminal domain containing a MT-binding domain (Dehmelt and Halpain 2004). MAP2 and tau are expressed in neurons while MAP4 is expressed additionally outside the CNS (Chapin, Bulinski, and Gundersen 1991). The Tau protein is encoded by a single gene, spanning 16 exons (Neve et al. 1986), and through

alternative splicing of exons 2, 3, and 10, six isoforms are generated in human brain (Goedert and Jakes 1990). Further splicing of exons 4A and 6 in neurons of the PNS give rise to additional tau isoforms referred to as high molecular weight tau (Couchie et al. 1992). The expression of the different isoforms is tissue specific and is regulated during development according to the function required for cytoskeletal plasticity during synaptogenesis and neurite outgrowth (Nunez and Fischer 1997). In the adult brain tau was found predominantly bound to MTs in the neuronal axon, promoting tubulin polymerization and stabilizing MTs (Weingarten et al. 1975; Drechsel et al. 1992). Throughout the last decades it was suspected that tau has a stabilizing function, supporting the extended structure of the long axon and through its interaction with stable domains of MTs and therefore affecting morphogenesis, differentiation, neurite polarity, axon elongation and outgrowth, and motor protein-mediated axonal transport (Esmaeli-Azad, McCarty, and Feinstein 1994; Samsonov et al. 2004; Dixit et al. 2008; Dawson et al. 2010). Using FRET analysis it was shown that tau interacts via discrete distribution on so called hot spots with MTs (every 60 tubulin dimer) (Breuzard et al. 2013). Further studies from another group showed that tau hops between MT neighbors, interacting with an average dwell time of ~ 40 ms to each MT spot, called the kiss-and-hop-kinetics of tau proteins (Janning et al. 2014). In 2018 however, Qiang showed that, opposite to the previous theory about tau-MT stabilization, tau is not a stabilizer of MTs (Qiang et al. 2018; reviewed by Baas and Qiang 2019) but rather it is enriched on labile domains along the axonal MTs allowing them to have even longer labile domains. In the absence of tau it could be seen that other stabilizing proteins, such as MAP6, are expressed highly and bind more effective to the labile domains and therefore having a stabilizing function on the axonal MTs (reviewed by Baas and Qiang 2019).

Based on its functional versatility it is not surprising that tau is involved in many neurodegenerative disorders. Most of these diseases are characterized by intracellular aggregations of proteins, with tau among them, forming intracellular fibrillary deposits in neurons and glial cells. Diseases characterized by tau aggregations are called tauopathies. The precise mechanism how tau is involved in neurodegenerative diseases is not yet known. Generally, tauopathies are categorized into two classes depending on whether tau is considered the major disease-coursing factor or not (Williams 2006; Dickson et al. 2011). One well-

known neurogenerative disorder is Alzheimer's disease (AD), where tau was found in a hyperphosphorylated state. In normal tissue, tau has 2-3 moles phosphate/mole of tau protein. In an AD brain, tau is three to four times higher phosphorylated, which leads to neurofibrillary tangle formation where paired helical filaments (PHF) are mixed with straight filaments (Iqbal et al. 2010). Most studies on tau concentrated on its dysfunction occurring through protein modifications such as hyperphosphorylation (Trinczek et al. 1995).

Intermediate filaments

IFs receive their name from their diameter, which is between that of MTs and microfilaments. Their large number, diverse primary structure, nonpolar architecture, distribution to the cytoplasm and nucleus, and their relative insolubility are properties that differ from actin microfilaments and MTs. At least 65 functional genes of the human genome are encoding IF proteins and as many as 30 diseases are related to mutations in these genes.

IF proteins are classified into 6 categories, based on their amino acid sequence similarities. Keratins belong to type I and type II IF proteins (acidic keratins and neutral basic keratins). Vimentin, desmin, peripherin and glial fibrillary acidic protein (found in muscle cells, white blood cells, fibroblasts and glial cells) form type III IFs. Type IV IF proteins include the three NF subunit proteins NF-L, NF-M and NF-H (for light, medium and heavy), which are prominent in many types of mature neurons. Nuclear lamins considered type V IF proteins (found in most eukaryotic cells), while nestin is classified as type VI IF protein.

The various IF proteins exhibit a common structural organization. All of them have a central α-helical rod domain (consisting of about 310 amino acid residues) which is flanked by N- and C-terminal globular and unfolded domains. The flanking regions of the different IF protein types vary in size, sequence and secondary structure. The filaments assemble by first winding the central rod domains of two polypeptide chains around each other into a coiled-coil structure. Dimers then associate to form tetramers, in a staggered antiparallel fashion. The final filament consists of eight protofilaments wound around each other in a rope-like fashion. As the basic subunits of the filaments represent antiparallel

tetramers, the final filaments possess equally structured ends and thus are non-polar.

NFs, the IF type of interest in this thesis, are important for providing mechanical stability to the axon and establishing its diameter. For the maturation of axons and the fulfilment of its functions, such as correct transmission speed of electrical signals, it is important that the longest axon has the proper diameter. The bigger the diameter, the faster the signal transmission. Furthermore, NFs are interlinked with MTs that are aligned with them along the axon. Of foremost importance for this interlinkage are proteins of the plakin family (see below) that interconnect IFs with MTs as well as actin filaments, producing a reversibly cross-linked filamentous meshwork.

NF polymers are synthesized in the cell body and transported into the axon along MTs in short cycles of fast movement interrupted by short pausing times (Brown, Wang, and Jung 2005). For a long time it was not clear whether NFs are transported via slow or fast axonal transport, Wang and Brown (2001) published that NFs are transported via fast axonal transport interrupted by prolonged pausing times leading to an average velocity of NF transport of about 0,5 µm/s excluding pauses. To sum up, the slow rate of movement measured is based on the average of rapid bidirectional movement and prolonged pauses. These findings led to a stop- and-go hypothesis of slow axonal transport. Further research revealed 2005 that NFs are found in two states, an on-track and an off-track state. In an on-track state NFs are moving along the MTs in a fast manner with only short pausing times while off-track NFs are disengaged from the MTs leading to long pausing before further connection and movement (Brown, Wang, and Jung 2005).

Plectin: functions and molecular properties

Plectin, a huge (>500 kDa) cytoskeletal crosslinking protein, is widely expressed in all types of mammalian cells. The protein belongs to a superfamily of proteins called plakin or simply cytolinker protein family. The members of this family associate with various cytoskeletal elements and junctional cell complexes. Seven plakin family members are known by now: Desmoplakin, bullous pemphigoid antigen 1 (BPAG1), MT-actin crosslinking factor (MACF, alias ACF7),

envoplakin, periplakin, epiplakin, and plectin. Of these, plectin is the best studied family member.

Plectin´s versatility as cytoskeletal linker is based on its multidomain structure providing specific interaction sites for all of the three major cytoskeletal filament systems (see above). Plectin functions as a stabilizer for cells by networking and anchoring IFs to organelles and junctional complexes (reviewed in Wiche and Winter 2011; reviewed in Castañón et al. 2013). Additionally, it regulates cytoskeleton dynamics and plays an important role as cytoplasmic scaffolding platforms for signaling cascades, controlling dynamic and metabolic activities of cells. Plectin binds directly to IF ptoteins such as vimentin, glial fibrillary acid protein, NFs, desmin, lamin B and type I and II keratins (Foisner et al. 1988, Reipert et al. 1999, Steinböck et al. 2000). In earlier studies it was shown that plectin mechanically links IFs to cytoskeletal structures such as the subplasma membrane skeleton, Z-disks of myofibers, mitochondria and the nuclear lamina (reviewed in Wiche, Osmanagic-Myers, and Castañón 2015). Furthermore, early on it was shown that plectin-IF interactions are regulated by phosphorylation, such as the dissociation of vimentin through phosphorylation by protein kinase C (Herrmann and Wiche 1987; Foisner and Wiche 1991) in addition to its interaction with IFs, plectin interacts with actin filaments and MTs.

As shown in Fig. 6, plectin has a tripartite structure consisting of two globular N- and C-terminal domains and an ~200 nm long coiled-coil rod domain. The plectin gene spans over 62 kb and comprises over 40 exons. The central rod domain is encoded by a single large exon, exon 31. Similarly, the C-terminal domain (~200 kDa) is encoded by a single exon (exon 32) containing six repetitive sequences (repeat domains R1-R6) connected by linker sequences (Wiche et al. 1991). Plectin´s universal IF-binding domain is located between R5 and R6. The N terminus of plectin, encoded by the remaining >30 exons, has the remarkable feature that multiple alternative first exons are spliced into a common exon 2. Exons 2-8 encode the actin-binding domain (ABD) of plectin (Sevcík et al. 2004). Two small exons, 2α and 3α, located within the ABD are optionally spliced in the exons 2 and 4 (see Fig. 7). Exons 9-30 encode for the so called plakin domain of plectin (Fig. 6). Plectin interacts with other proteins via its Scr-homology 3 (SH3) domain located toward the middle of the plakin domain. SH3 domains are known

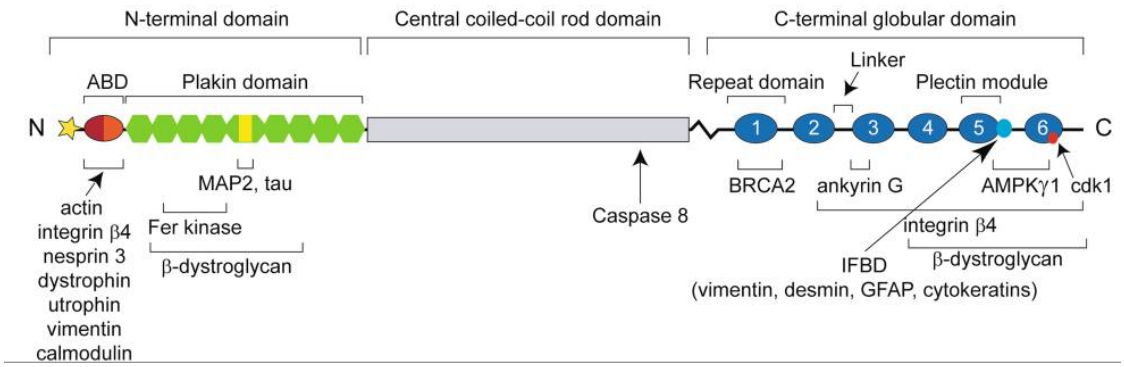

Figure 6. Schematic representation of the plectin molecule

The protein structure is built up of 3 major domains: An N-terminal globular, a central coiled-coil rod, and a C-terminal globular domain. In the N-terminal domain an actin-binding domain (ABD) is located, consisting of two calponin homology domains (dark and light red), and a plakin domain comprising nine spectrin repeats (green) and one SH3 domain (yellow). The central rod domain has a coiled-coil structure with a length of 200 nm. The C-terminal domain contains six conserved repeat domains (blue) connected through linker regions, one of which harbors the IF-binding domain (*IFBD*, light blue). The various N termini of the different isoforms are marked by a yellow star. Bellow the scheme the positions of mapped binding regions to various proteins are shown. Image and legend from Castañón et al. 2013

to mediate protein-protein interactions, binding to proline-rich sequences (Kaneko, Li, and Li 2008). In a recent report it was shown that plectin binds to MAPs, such as MAP2 and tau, via its SH3 domain and thus antagonizes MAP mediated MT stabilization, leading to MT destabilization (Rocio G Valencia et al. 2013).

Plectin Isoform diversity

Alternative splicing at the 5`end of the plectin gene leads to a variety of transcript variants (Fig. 7). Twelve alternative first exons, named E1 to E1k, are spliced into a common exon 2, three of them being non-coding (Eh, Ei, Ej). Exon 1c is preceded by three non-coding exons (E0, E0a and E-1), and within the exons encoding the ABD (exon 2-8), two additional short sequences encoded by exons 2α and 3α can be found in some transcripts (Fuchs et al. 1999). This large variety of alternative splicing events gives rise to a series of isoforms with distinct binding specificities, which are responsible for different isoforms being targeted to different cellular structures, such as focal adhesions (FAs), hemidesmosomes

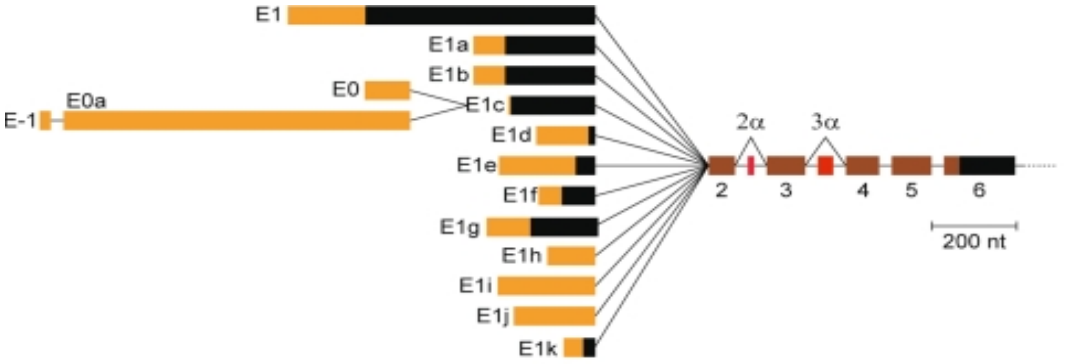

Figure 7. Plectin isoform diversity

Transcripts generated by alternative splicing of the 5′ end of the gene. Exons are indicated by *boxes*, *orange* areas within the *boxes* denote noncoding regions, *black* areas, coding regions. *Brown boxes* indicate coding sequences if preceded by one of the first coding exons (*1-1 g*, *1 k*), or noncoding sequences if preceded by one of the noncoding exons (*1 h-1j*). The *black* area within exon *6* denotes the first coding region of transcripts starting with exons *1 h*, *1i*, and *1j*. Two optionally spliced exons inserted between exons *2* and *4* are shown in *red*. Image and legend from Castañón et al. 2013.

(HDs), MTs, mitochondria, and Z-disks (Rezniczek et al. 2003).

As all isoforms are endowed with a high-affinity IF-binding site at their C-termini, plectin is able to control the cytoarchitecture of IF networks and thereby affect basic and cell type specific features of cells (Wiche and Winter 2011). The expression patterns of the different isoforms in various cell types were revealed by RNase protection assays, using antisense riboprobes specific for all the first exons (Fuchs et al. 1999). Except for isoform P1d all other plectin isoforms were found in all types of tissue tested including lung, brain, muscle, skin, liver although some isoforms showed low levels of expression in certain tissues. P1a, P1b, P1c, P1d, and P1f in general showed higher expression levels compared to the other transcript variants. P1c was the isoform dominantly expressed in brain tissue as well as skin.

From early on it was proposed that plectin plays an important role in IF network organization interlinking all types of IFs (Wiche and Baker 1982; Foisner et al. 1988) and regulating IF dynamics (Steinböck et al. 2000). It was observed that in the absence of plectin the IF networks of fibroblasts phenotypically show a less compact and more extended organization compared to WT cells. Further, while it seems that in WT cells plectin anchors vimentin at the center of the cell, in plectin$^{-/-}$ fibroblasts vimentin was not restricted anymore to the central part

(reviewed by Wiche and Winter 2011). In skeletal muscle fibers, plectin has been shown to associate with desmin filaments, interlinking them to mitochondria and neighboring myofibrils (Andrä et al. 1997; Reipert et al. 1999). Progressive degenerative alterations of the desmin network could be observed in plectin KO mice, such as aggregation and partial loss of desmin IFs (Konieczny et al. 2008). Another cell type where the IF interacting and crosslinking function of plectin was observed are keratinocytes. Here, similar to vimentin in fibroblast, keratin filaments could be found to be more bundled and less flexible when plectin is not expressed. Further, the IF networks in keratinocytes were extending to the periphery while in WT cells a filament-free zone at the periphery could be observed (Osmanagic-Myers et al. 2006). One of the isoforms expressed in keratinocytes is P1a, which binds specifically to integrin $\alpha 6\beta 4$, thus interlinking the IF network system with the extracellular matrix. This linkage plays an important role in the assembly and disassembly of HDs. P1c, the plectin isoform I have been working with in this thesis, is the second major isoform expressed in keratinocytes (Andrä et al. 2003). It shows a destabilizing effect on MTs as will be described in more detail below.

Plectin isoform 1c

As the role of P1c in neuronal cells was the topic of my thesis, in this chapter I will give a more detailed overview on this particular isoform. The first plectin gene to be cloned and sequenced was from rat (Wiche et al. 1991), while the human gene was cloned 5 years later (Liu et al. 1996). The first four splice variants generated by alternative splicing of 1st coding exons (E1, E1a, E1b, and E1c) of the plectin gene were then identified in rat (Elliott et al. 1997). Studying the expression of P1c transcripts in different tissues, it was found that P1c is expressed at high levels in brain and skin (Fuchs et al. 1999; Andrä et al. 2003).

Later it was found that P1c is widely expressed throughout the whole nervous system, particularly at late developmental stages (Fuchs et al. 2009). In mouse brain, P1c was found in all grey matter areas, and in the cerebral cortex, in all cortical layers, with strongest expression in the outer granular layer. Furthermore, expression of P1c was detected in neuronal dendrites, in motor

neurons and smaller interneurons of the spinal cord, in peripheral areas of axons and in the cytoplasm of Schwann cells, but not in myelin sheaths.

To sum up, P1c is expressed at high levels in neuronal tissues and epithelia, which is not surprising as both types of tissues share a common developmental origin, the ectoderm. While little is known about the functions of P1c in neurons, P1c´s role in keratinocytes has been studied in some detail. Valencia et al. (2013) reported that P1c deficiency alters the MT network of keratinocytes. Keratinocytes derived from newborn plectin KO (P-zero/P0) mice displayed more densely packed MT bundles compared to WT cells and confocal immunofluorescence microscopy showed that P1c colocalized with MTs in a dotted pattern. Upon treatment with nocodazole, a MT-depolymerizing drug, MTs were found to be more resistant towards disassembly and thus considered more stable in P1c-deficient keratinocytes compared to their WT counterparts (Valencia et al. 2013). Furthermore, consistent with the observations that stable MTs usually show a higher degree of α-tubulin acetylation (Piperno, LeDizet, and Chang 1987; Bulinski, Richards, and Piperno 1988), increased levels of acetylated α-tubulin were found in plectin-deficient keratinocytes (Valencia et al. 2013). These observations suggested that P1c acts as a MT destabilizer, altering the dynamic behavior of MTs with consequences for the shape and directional migration of cells (Valencia et al. 2013).

Reports on the influence of P1c on the cytoskeleton network of neuronal cells are rare. In a first study on P1c-deficient mice, a significantly reduced conduction velocity was observed in sciatic nerves, and in phrenic nerves of KO animals the neurons exhibited a higher proportion of axons with small cross-sectional areas, correlating with the observations of reduced conduction velocity (Fuchs et al. 2009). Additional biochemical studies using brain lysates revealed that plectin (presumably P1c) binds at least one of the HMW MAPs, via its SH3 domain (Valencia et al. 2013). Furthermore, it was shown that the minimum fragment required for MAP-binding (p20-21, see below) can compete with MTs for binding to tau, thereby preventing the interaction of MAPs with tubulin.

Plectin´s role in disease - plectinopathies

Plectinopathies are caused by mutations in the human plectin gene (*PLEC*) located on chromosome 8. The most common disease known is epidermolysis bullosa simplex with muscle dystrophy (EBS-MD), which is a rare autosomal skin blistering disorder manifesting with severe skin and mucous membrane blistering and late-onset muscular dystrophy (Gache et al. 1996; Smith et al. 1996). Further plectin mutations were identified in multiple other diseases, such as EBS-MD in combination with a myasthenic syndrome (EBS-MD-MyS) (Banwell et al. 1999; Forrest et al. 2010), EBS with pyloric atresia (EBS-PA) (reviewed by Rezniczek, Walko, and Wiche 2010; Natsuga et al. 2010), and limb-girdle muscular dystrophy type 2Q (LGMD2Q) (Gundesli et al. 2010). Furthermore, a dominant mutation in plectin has been found to cause the rare skin blistering disease EBS-Ogna (Koss-Harnes et al. 2002). Typically, EBS-MD plectinopathies are characterized by desmin-positive aggregates, mitochondrial abnormalities, and myofibril degeneration and consequently are classified as myofibrillary myopathies (Schröder and Schoser 2009; Winter and Wiche 2013). Some EBS-MD and EBS-MD-MyS patients show signs of neurodegenerative disorders, leading to the hypothesis that the expression of defective plectin or the complete absence of an isoform may also cause neuropathies (Smith et al. 1996).

Another disease where plectin deficiency plays a role is Alexander disease. In this case, patients suffer from episodes of severe seizures and macroencephaly, leading to progressive disability or early death (Tian et al. 2006). Here the low amount of expressed plectin leads to the aggregation of GFAP, an astrocyte-specific IF protein.

Aim of the thesis

The goal of my thesis was to investigate the function of P1c in neurons. The idea was to isolate two types of neurons, DRG and hippocampal neurons, from WT mice and compare their functional properties with those of their counterpart neurons from plectin-null and plectin isoform P1c-deficient mice. Mouse lines of the latter type had been established and subjected to various analyses in previous studies at my host laboratory.

The first question to be addressed was what happens to the NF network system in the absence of P1c. Based on previous studies performed with keratinocyte hypothesized that P1c deficiency alters the anchoring of NFs, the shape and distribution of the filaments and possibly the transport of NFs along MTs. Other questions to be answered were whether P1c binds to neuronal MTs in an isoform specific manner and whether it has a MT destabilizing function in neurons similar to its previously reported action in keratinocytes. In the case I would find a MT-related phenotype, experiments were planned to gain insights into its underlying mechanism. In particular, it would be of interest to assess whether P1c prevents the binding of tau proteins to neuronal MTs, which may lead to more MT-bound tau in the absence of P1c, and consequently to alterations in MT dynamics. A final goal was to investigate whether P1c deficiency affects structural and/or functional features of neurons that are known to be MT-dependent, such as morphology, growth cone formation, neurite outgrowth, and axonal branching.

Results

This section of the thesis is subdivided into 3 parts addressing the functional role of plectin isoform P1c in two neuronal cell systems: DRGs and hippocampal neurons. First the importance of P1c for the organization and function of the NF system is described, while in the second part the targeting of P1c to MTs and its effects on MT properties is shown. In part three, physiological alterations in neurons stemming from P1c deficiency are described.

Most results gained in this thesis are contributing to a paper published in June 2020 “Plectin dysfunction in neurons leads to tau accumulation on microtubules affecting neuritogenesis, organelle trafficking, pain sensitivity and memory“ published by R. G. Valencia, E. Mihailovska, L. Winter, K. Bauer, I. Fischer, G. Walko, J. Jorgacevski, M. Potokar, R. Zorec, G. Wiche.

Establishment of optimal conditions for DRG and hippocampal neuron isolation

As the systems to be studied in this thesis were DRG and hippocampal neurons, it was essential to establish optimal conditions for culturing these cell systems. A protocol for isolating and culturing DRG neurons from mice previously established in the lab had to be modified with respect to minor points, such as minimizing the time frame from scarifications of mice to single cell preparation and cell lysis down to 30-40 minutes, which was especially important for the MT-binding assay (see detailed protocol in chapter Materials and Methods).

For the isolation and culture of hippocampal neurons, no detailed protocol had previously been established in the lab. For first tests, I followed the experimental protocol of Seibenhener and Wooten (2012) in combination with the protocol of Zeitelhofer (2007). Instead of prenatal mice (embryonic days 15 or 19) as used by these groups, I used newborn (day 0) mice for isolation of hippocampal cells. The reason was that P1c is expressed at late developmental stages, so I wanted to have fully developed brains to distinguish between WT and P1c$^{-/-}$ hippocampal neurons. Different to the previous protocols, the coverslips for culture were coated with poly-L-lysine (PLL) instead of poly-D-lysine (PDL),

following the recommendations of the supplying company (see Materials and Methods) and on basis of our own experience with DRG neurons. Isolation of brain and sectioning of hippocampi were performed outside the laminar hood in a sterile 3.5 cm petri dish in pre-warmed solutions (HBSS) under a microscope. To maintain sterile conditions, the instruments were cleaned with 70% ethanol and autoclaved before use. The surfaces of the microscope were cleaned carefully with ethanol each time and the time frame for working outside the hood (from killing the animal to submerging the hippocampi in sterile HBSS) was minimized to 5 min. After that, all further steps were done under sterile conditions following the protocol of Zeitelhofer (2007).

As the genotyping of mice could not be done before hippocampal cells had been to be isolated, hippocampal neurons were isolated from all pups of a litter and the genotyping was done afterwards. According to Zeitelhofer´s protocol for transfection of hippocampal neurons, it was suggested to use $6x10^6$ cells for one nucleofection reaction. Anyway, to gain as many neuronal cells in culture as possible and reduce the number of pups needed, the hippocampi of one pup were triturated in 2 ml and then divided into 3 equal volumes. One third, used as control, was centrifuged and cells resuspended in 2 ml pre-warmed plating medium, and 1 ml of cell suspension was seeded on a coverslip of a 24 well plate. The other two thirds were used for nucleofection with different plasmid DNAs. Further steps for transfection were continued according to Zeitelhofer (2007) As the mixing of the DNA with cells seemed to be a critical step, I cut off the tips of yellow pipette tips to gain a wider opening and be able to mix slowly and very gentle without damaging the cells.

The scheme shown in Fig. 8A shows the different steps I took to successfully establish a hippocampal cell culture, from the isolation and dissection of hippocampi to the preparation of single cell suspensions, followed by nucleofection.

A preliminary test with an expression plasmid encoding a truncated version of P1c (P1c20-21-GFP) showed that hippocampal neurons isolated in such a way, could be transfected with reasonably high rates (about 40%, data not shown). As a further control, transfected cells were subjected to immunofluorescence microscopy using antibodies to actin (red) and tau (blue), establishing optimal conditions for immunostaining Fig. 8B.

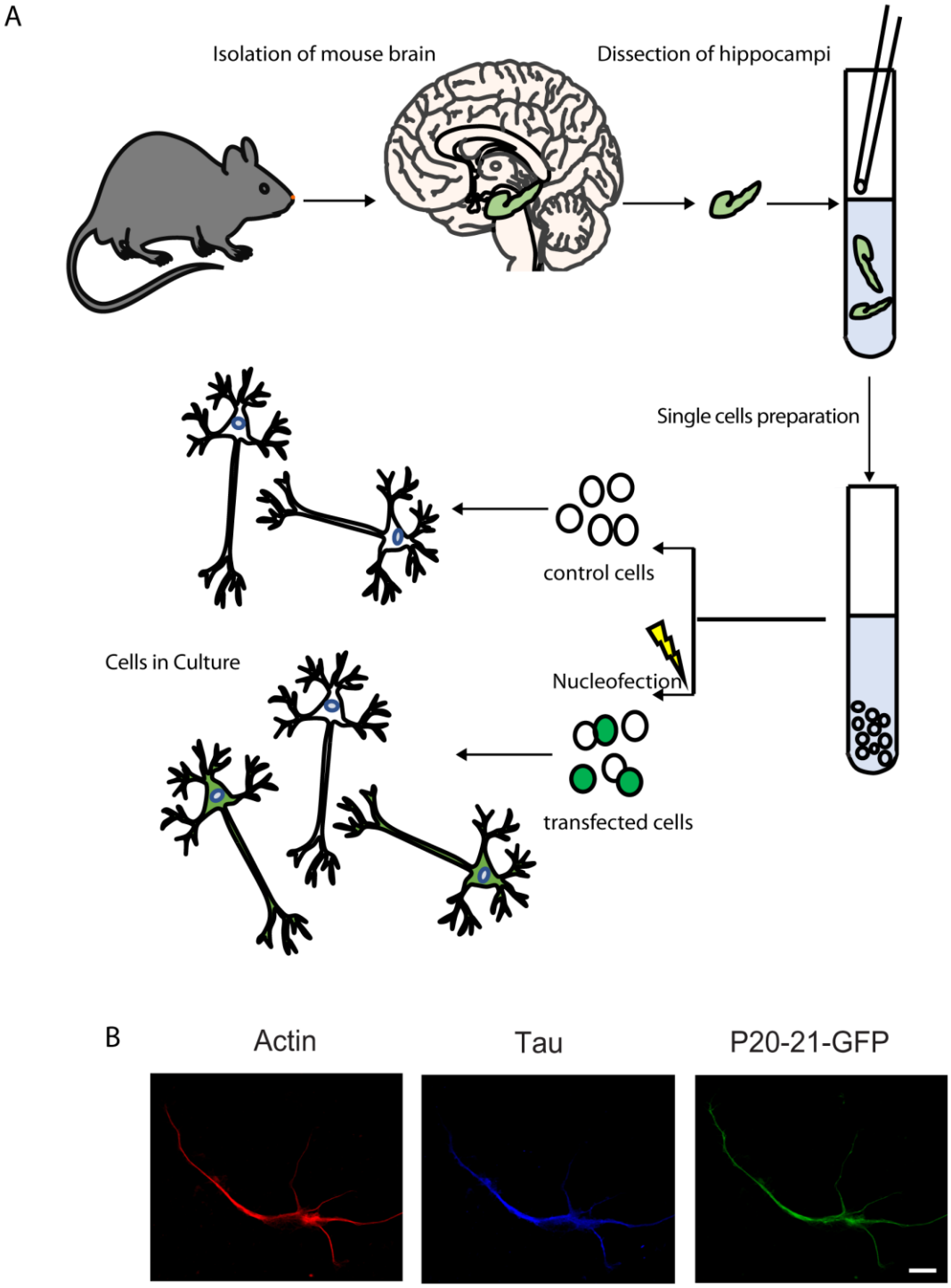

Figure 8. Scheme of hippocampal cell cultivation and transfection

(A) Hippocampal neurons were isolated from newborn (day 0) P1c$^{-/-}$ mice. Cells were lysed and transfected using "Lonza Nucleofection Kit" before cultivation. **(B)** Microscope images of cells first transfected with a plasmid (P1c20-21-GFP) encoding a truncated version of P1c and then immunolabled with antibodies to actin (red) and tau proteins (blue). Scale bar, 10 μm.

P1c deficiency affects NF network organization and dynamics

As NFs are the major IF type expressed in neuronal cells and P1c is the major isoform expressed in brain tissue, it was of great interest to investigate the impact of P1c on the NF cytoskeleton network. It has previously been shown that plectin interacts with all three of the NF subunit proteins, NF-H, NF-M, and NF-L (Foisner et al. 1988). To investigate, whether P1c deficiency alters NF network organization and/or dynamics, primary DRG neurons isolated from 8 week-old P1c$^{-/-}$ and WT littermate mice were subjected to immunofluorescence microscopy using antibodies to NFs and additionally labeled with Texas-Red-coupled phalloidin to visualize the actin cytoskeleton in growth cones. Immunostained NFs in WT DRG neurons showed a bundled and often ring-like structure, located near the neck of the axon shaft (Fig. 9A). In P1c$^{-/-}$ DRG neurons, NFs seemed to have a more dispersed appearance, distributing out of the axon in a fan-like fashion and penetrating deeply into the growth cone (Fig. 9A). Statistical evaluations of growth cones harboring ring-like NF structures revealed that about 59% of WT growth cones showed NFs with a ring-like structure, whereas only about 12% of P1c$^{-/-}$ cells showed a similar structure (Fig. 9C). A fan shaped structure with deep penetration into growth cones could be analyzed in more than 79% of P1c$^{-/-}$ neurons. Moreover, when the penetration depth of NFs protruding into the growth cones was analyzed by manual tracking with ImageJ, P1c$^{-/-}$ neurons showed a ~1.7 fold increase of NF penetration depth compared to their WT counterparts (Fig. 9D). Lastly, a semi-quantitate analysis of NF levels was performed by measuring the fluorescence intensity (pixel count) in growth cones. For evaluation, the images were analyzed with Image J, tracking the growth cones and NF areas manually and measuring the pixel intensities per growth cone area. Consistent with the visual appearance, the fluorescence intensity of NFs per growth cone area was drastically reduced in P1c$^{-/-}$ neurons compared to WT cells, the latter showing a ~2.7-fold higher intensity (Fig. 9B). Typically, NFs move bidirectionally in an intermittent manner (Watson, Glass, and Griffin 1993; Glass and Griffin 1994), existing in an on track and off track state (Brown, Wang, and Jung 2005). NF subunit proteins are synthesized in the cell body and transported

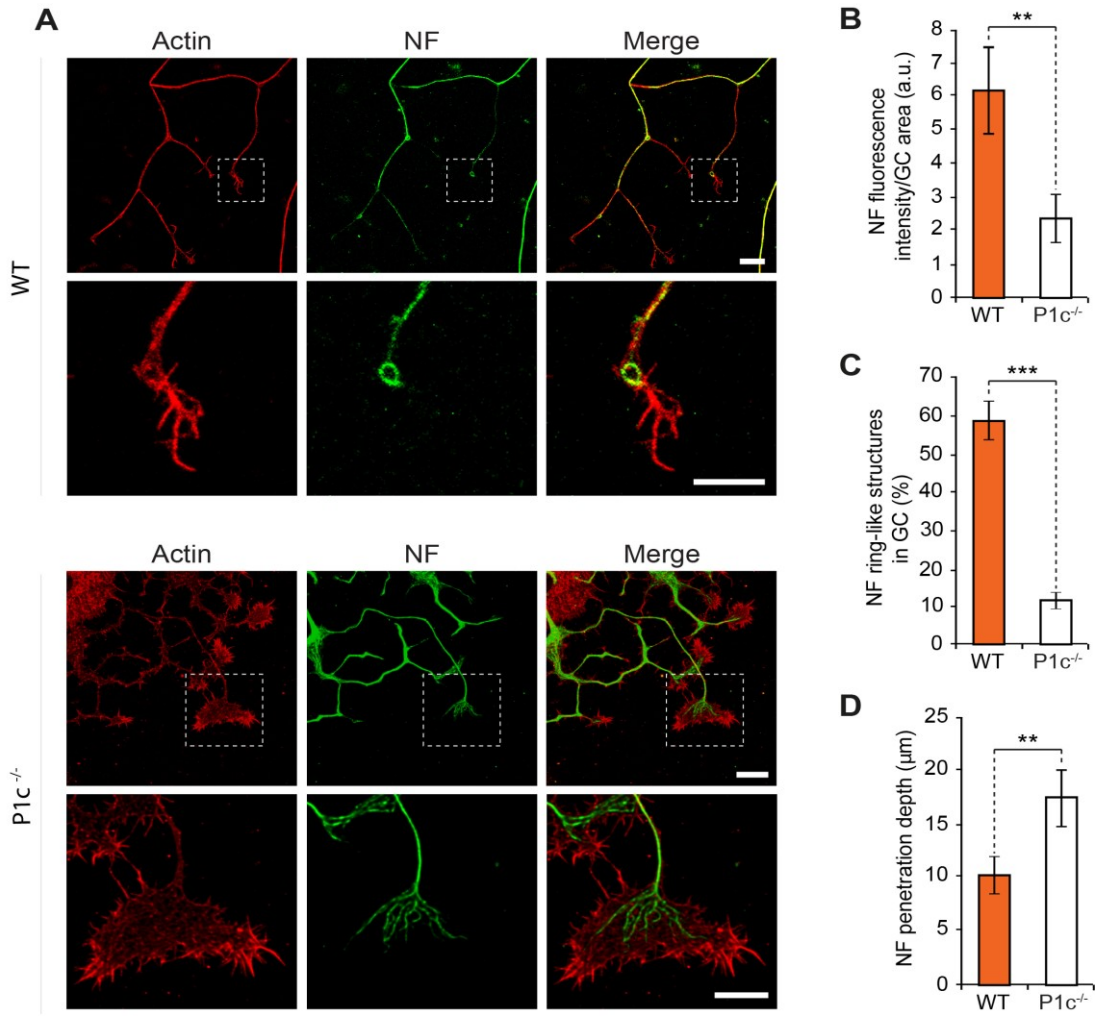

Figure 9. Lack of P1c affects NF network organization of DRG neurons

(A) Visualization of NF and actin networks in WT and P1c$^{-/-}$ DRG neurons using antibodies to NFs and Texas Red-X phalloidin for actin. Boxed areas (upper panels) are shown at higher magnification in lower panels. Scale bars, 10 µm (upper panels), 5 µm (lower panels). Note ring-like NF structure at the axon-growth cone transition area in WT neurons, contrasting the fanning out and deeper penetration of NFs into the P1c$^{-/-}$ growth cone. **(B)** Semi-quantitate analysis of NF intensities per pixel. Mean ± SEM (WT n=21, P1c$^{-/-}$ n=18) **(C)** Percentage of growth cone displaying ring-like NF structures. Mean ± SEM [WT (n=44), P1c$^{-/-}$ (n=42)]. **(D)** Quantification of NF growth cone-penetration (distance between growth cone start and furthermost tip of NFs). Mean ± SEM [axons analyzed: WT (n=21), P1c$^{-/-}$ (n=18)]. P-values **<0,01, and ***<0.001

via rapid movement, retro- and anterogradely along the axon by motor proteins. According to the stop and go hypothesis, NFs are supposed to spend only ~8% of their time “on track” and ~96% in an “off-track” state showing longer pausing times than moving (Brown, Wang, and Jung 2005).

In light of the observed alterations in NF network organization, it was of interest to obtain more information about the molecular dynamics of NFs in WT compared to P1c$^{-/-}$ DRG neurons. For this, time-lapse microscopy was performed, following the protocol of Uchida and Brown (2004), where WT and P1c$^{-/-}$ DRG neurons were transfected with expression plasmids encoding a GFP-tagged version of the NF subunit protein NF-M. GFP-tagged NF particles, moving anterogradely or retrogradely into an area of the axon that had formerly been bleached, were monitored by video microscopy in a time frame of 10 minutes. Fig. 10A shows the retrograde movement of a 3 µm-long NF particle into the bleached area of an axon at time points 0, 16, 28 and 124 seconds after bleaching.

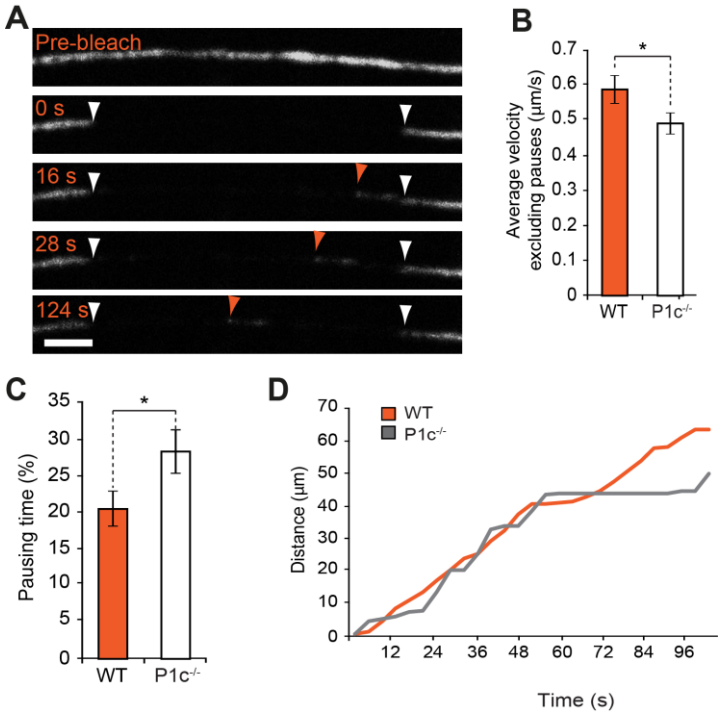

Figure 10. P1c deficiency leads to reduced NF transport in DRG neurons

Visualization of GFP-tagged NF particles moving along axons within a photobleached area. Images were selected at different time points (pre-bleach; 0, 16, 28 and 124 seconds after bleach) from a time-lapse movie. White arrowheads, borders of the bleached zone. Orange arrowheads, retrogradely moving particles. Scale bar, 5 µm. **(B)** Statistical analysis of average velocity of moving NF particles excluding pausing times. Mean ± SEM (particles analyzed: WT n=49; P1c$^{-/-}$ n=47). **(C)** Evaluated pausing time of NF particles during movement. Mean ± SEM (particles analyzed: WT n=45; P1c$^{-/-}$ n=47). **(D)** Graph of NF particle movement along axon in WT and P1c$^{-/-}$ neurons. Y-axis, distance moved. X-axis, time phases of movement and pausing of particles appearing in bleached area. P-values *<0.05

Analyzing the mobility of several NF particles it became apparent that in P1c$^{-/-}$ neurons particles moved slower (0.45 µm/sec without pausing time) compared to WT particles (0.59 µm/sec) (Fig. 10B). Moreover, NFs were not only transported at a slower rate in P1c$^{-/-}$-deficient cells than in their WT counterparts, but they also paused more often. Whereas, in P1c$^{-/-}$-deficient neurons NF particles were observed as immobile during 28% of the recording time, in WT neurons the corresponding proportion amounted to only 20% (Fig. 10C). Furthermore, as visible in Fig. 10D, WT particles moved faster and with shorter pausing times along the axon shaft compared to their P1c$^{-/-}$ counterparts, which sometimes stopped up to 144 seconds before moving again (data not shown). In conclusion, NF particles move slower and make more stop and go pauses in P1c$^{-/-}$-deficient DRG neurons compared to their WT counterparts.

Colocalization and isoform-specific targeting of P1c to axonal MTs

In previous studies with keratinocytes, it was found that P1c deficiency affects MT stability and dynamics with consequences for MT-dependent functions (Valencia et al., 2013). To examine whether P1c co-localizes with MTs in neuronal cells, I performed double immunofluorescence microscopy of cultured DRG neurons isolated from WT mice using isoform-specific antibodies to P1c and anti-α tubulin antibodies. As shown in Fig. 11, P1c was found in close association with MTs along the neurite shaft as well as in the growth cone.

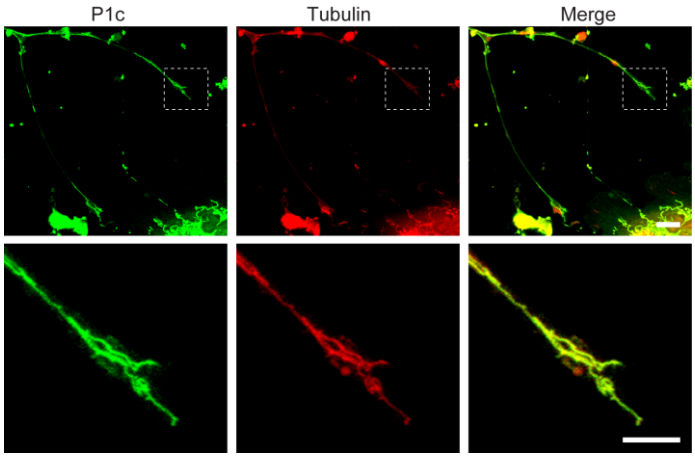

Figure 11. Co-localization of P1c with axonal MTs

(legend on page 42, bottom)

To assess whether the association of P1c with MTs in neurons was isoform specific, I first transfected WT DRG neurons with expression plasmids encoding GFP-tagged full-length P1c (P1c(2α3α)-32-GFP) or a truncated version of P1c (P1c(2α3α)-8-GFP). Both expression plasmids contained neuron-specific sequences encoded by the two differentially spliced exons 2α and 3α. Immunostaining of transfected cells using specific anti-α tubulin antibodies showed that overexpressed P1c(2α3α)-32-GFP is co-localized with MTs all along theaxon as well as in the growth cone (Fig. 12A).

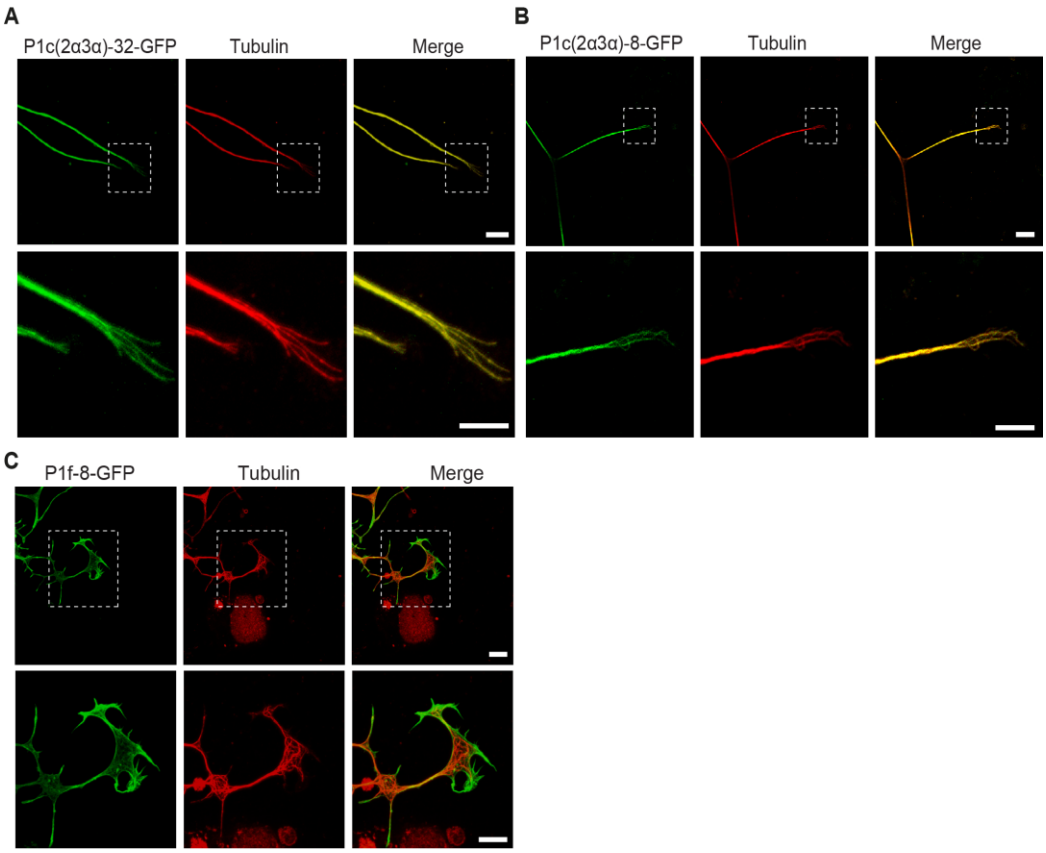

Figure 12. Isoform-specific targeting of P1c to MTs

WT DRG neurons transfected with P1c and P1f expression plasmids were immunolabled using anti-tubulin specific (red) antibodies. **(A-C)** cells were transfected with full-length P1c, truncated P1c, and truncated P1f, as indicated. Lower panels are magnifications of the boxed areas indicated in upper panels in the upper row. Scale bars, 10 μm (upper panels), 5 μm (lower panels). Note, both versions of P1c showed co-localization with MTs (yellow in merged images). Truncated P1f-8-GFP is detectable all along the periphery of the neuron, while MTs are in the middle of the axonal shaft and the growth cone are not targeted.

As shown in Fig. 12B, the truncated version P1c(2α3α)-8-GFP exhibited a distribution pattern that was very similar to that of the full-length version of P1c. To assess the specificity of P1c-binding, P1f-8-GFP, a similarly truncated version of plectin isoform P1f, was transfected into DRGs. P1f is an isoform that is prominently expressed at the plasma membrane and therefore was not expected to co-localize with MTs. Immunofluorescence microscopy of this truncated P1f version revealed a distribution along the whole neurite and at the periphery of the growth cone, while MT structures remained unlabeled (Fig. 12C). These results demonstrated that P1c binds to neuronal MTs in an isoform-specific manner.

P1c deficiency leads to increased levels of MT-bound tau in neuronal cells

In previous studies in vitro binding of plectin to MT-associated proteins (MAPs) has been demonstrated (Herrmann and Wiche, 1987) and P1c has been shown to antagonize MAP-binding to MTs by blocking the MAP-binding site on MTs (Valencia et al. 2013). Additionally, it could be shown that MT-stabilizing proteins are expressed in brain and in epithelial cells and tissues; tau plays also an essential role in axonal transport (Felgner et al. 1997; Stamer et al. 2002; Dixit et al. 2008). Recent research about tau-MT association showed that tau is not a MT stabilizer but rather enables MTs to have long labile domains and therefore supports MT dynamics (Qiang et al. 2018). In the present study, I wanted to investigate whether the lack of P1c in DRG and hippocampal neurons leads to an increase in endogenous MT-bound tau.

To visualize MT-bound tau proteins, DRG neurons from WT and P1c$^{-/-}$ mice were subjected to immunofluorescence microscopy using antibodies to tau and α-tubulin. To allow direct comparison, all images were taken below signal saturation and at equivalent intensities for WT and KO cells. As can be seen in

Legend to Figure. 11: Co-localization of P1c with axonal MTs

Double immunostaining of DRG neurons with P1c specific (green) and anti-tubulin (red) antibodies is shown. Lower images are magnification of the boxes in the upper row. Scale bars, upper row 10 µm; lower images 5 µm. The merged images reveal co-localization of P1c with MTs in the axonal shaft and in the growth cone.

Fig. 13A, P1c$^{-/-}$ cells appeared to have more tau bound along MTs compared to WT cells and they showed also higher signal intensities in axonal side branches. A semi-quantitive analyses of signal intensities, based on pixel counts, confirmed that in P1c-deficient cells more tau was bound along MTs compared to WT neurons (Fig. 13B). In fact, the tau to tubulin signal ratio, was 2.3-fold increased in P1c-deficient compared to WT neurons.

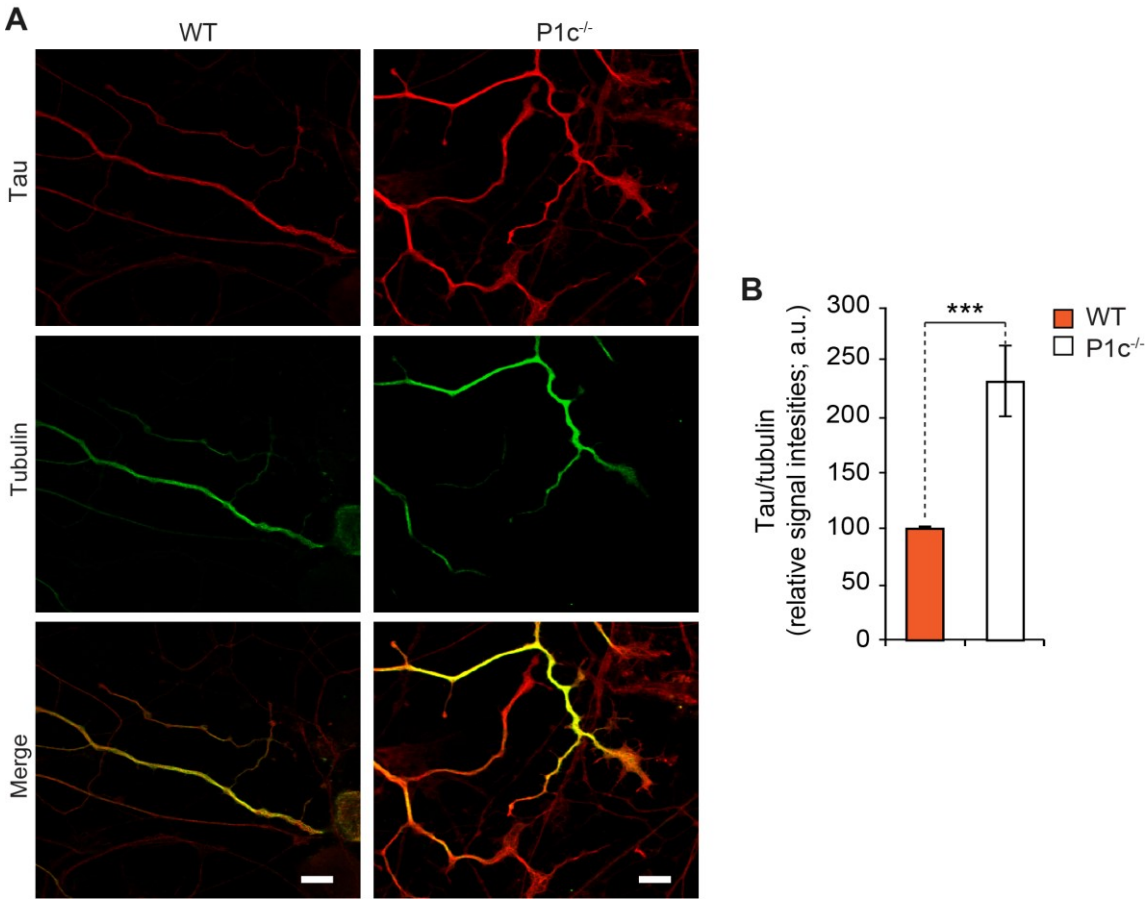

Figure 13. P1c-dependent association of tau protein with MTs of DRG neurons

(**A)** Confocal immunofluorescence microscopy of WT and P1c$^{-/-}$ DRG neurons using antibodies to tau and tubulin show increased tau signals in axons of P1c$^{-/-}$ compared to WT DRG neurons. Scale bars, 10 µm **(B)** The bar graph shows a statistical evaluation of tau-specific signal intensities normalized to tubulin signal intensity levels. Mean ± SEM (axons analyzed: WT n=105; P1c$^{-/-}$ n=93). P-value ***<0.001

To confirm that the lack of P1c was directly linked to increased MT-bound tau levels, rescue experiments were performed, where P1c$^{-/-}$ DRG neurons were transiently transfected with expression plasmids encoding GFP-fusion proteins of

full-length P1c (P1c-32-GFP), and the truncated versions P20-21-GFP (harboring the SH3 domain of plectin) and P16-24-GFP (SH3 domain plus preceding sequences). After transfection, the cells were immunolabeled for tau (red) and tubulin (green) to visualize their co-localization. Compared to the signal intensities measured in transfected cells, all of the fusion proteins expressed led to reduction of MT-bound tau (Fig. 14A).

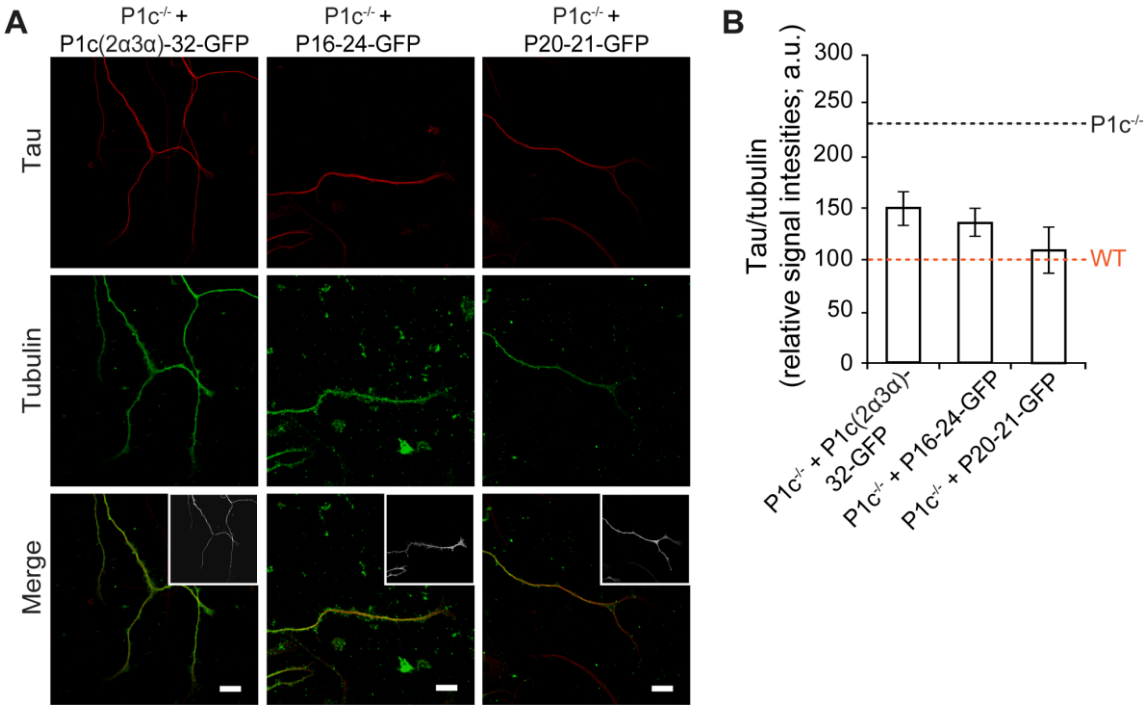

Figure 14. Rescue of MT-bound tau levels assessed by in situ localization

(A) P1c$^{-/-}$ DRG neurons were transfected with expression plasmids encoding C-terminal GFP fusion proteins, and immunolabled using antibodies to tau and tubulin. Transfected neurons were identified by their GFP-positive signals. Scale bars, 10 µm. Note, reduced tau-specific signal intensities in neurites upon transfection with any one of the three plectin expression plasmids tested. **(B)** Statistical evaluation of tau-specific signal intensities normalized to tubulin levels (all signals were recorded below saturation levels). Mean ± SEM. Axons analyzed: WT n=105; P1c$^{-/-}$, n=93; P1c$^{-/-}$+P1c-32, n=44; P1c$^{-/-}$+P16-24, n=101; P1c$^{-/-}$+P20-21, n=51. Note, transfection of P1c$^{-/-}$ neurons with full-length P1c or N-terminal plectin fragments P20-21 and P16-24 largely restored tau signals to WT control levels

Moreover, analyzing the tau to tubulin intensity ratios semi-quantitively (Fig. 14B) and comparing them to those of untransfected WT and P1c$^{-/-}$ cells (dotted lines in Fig. 14B) it became evident that the reduced levels of MT-bound

tau in transfected P1c$^{-/-}$ neurons nearly reached the level detected in untransfected WT cells. In particular, the ~230% increase in MT-bound tau observed in P1c$^{-/-}$ cells was cut down to ~148% in full length P1c-transfected cells, to ~136% in P16-24 transfected cells, and to ~110% in P20-21-GFP transfected cells.

To assess plectin-dependent tau association with MTs by an alternative approach, brain lysates were prepared from WT and P1c$^{-/-}$ mice under conditions where the polymeric state of MTs was maintained (Planel et al. 2008; Valencia et al. 2013). The endogenous MTs contained in such extracts, together with their bound proteins, were then sedimented by high speed centrifugation to obtain a MT-unbound and a MT-bound fraction. The levels of MT-bound and free tau protein in the different fractions, including the original cell lysate, were subsequently quantified by immunoblotting using antibodies to tau and α- tubulin. The immunoblots for tau and tubulin, and GAPDH (as loading control) are shown in Fig. 15A.

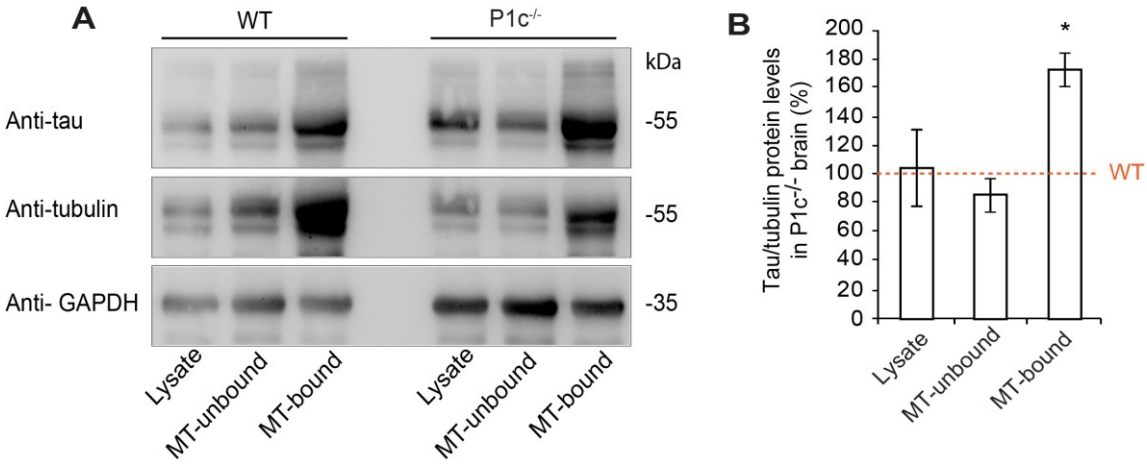

Figure 15. Plectin-dependent association of tau with intact MTs isolated from whole brain

A) Cell lysates prepared under MT-stabilizing conditions from WT and P1c-deficient mouse brain were fractionated, and total cell lysates, together with fractions containing MT-unbound, and MT-bound tau were analyzed by immunoblotting using antibodies as indicated. **(B)** Block diagram showing tau signal intensities normalized to tubulin levels. Mean ± SEM (n=3). P-value *<0.05

The major isoforms of tau expressed in brain (with an apparent molecular mass of ~50 kDa) and tubulin of nearly the same size were normalized to each

other, using the program “QuantiScan” for analysis and quantification. Comparing the tau to tubulin ratios determined for WT and P1c$^{-/-}$ lysates, P1c-deficient samples showed an increase of 175% of MT-bound tau compared to WT (Fig. 15B). Furthermore, in P1c$^{-/-}$ cells the amount of MT-unbound tau was found decreased by ~12%.

In a second approach, DRG neurons were isolated from 5 WT and 5 P1c$^{-/-}$ mice, fractionated and subjected to a similar co-sedimentation assay. In this case I monitored a tau variant of ~120 kDa, which is the most prominently expressed isoform in DRG neurons. Similar to the results obtained with brain lysates it was found that in P1c$^{-/-}$ cells the amount of MT-bound tau was significantly increased (up to ~900%) compared to its WT counterpart (Fig. 16B). In the total lysate only an up to ~210% increase of general tau signals could be detected and in the MT- unbound fraction the tau signal was ~90% increased compared to its WT counterpart. These data indicate that in the absence of P1c higher levels of tau proteins were bound to MTs, both, in cells isolated from whole brain as well as in freshly cultured DRG neurons. From this, one may conclude that P1c acts as an antagonizer of MAPs.

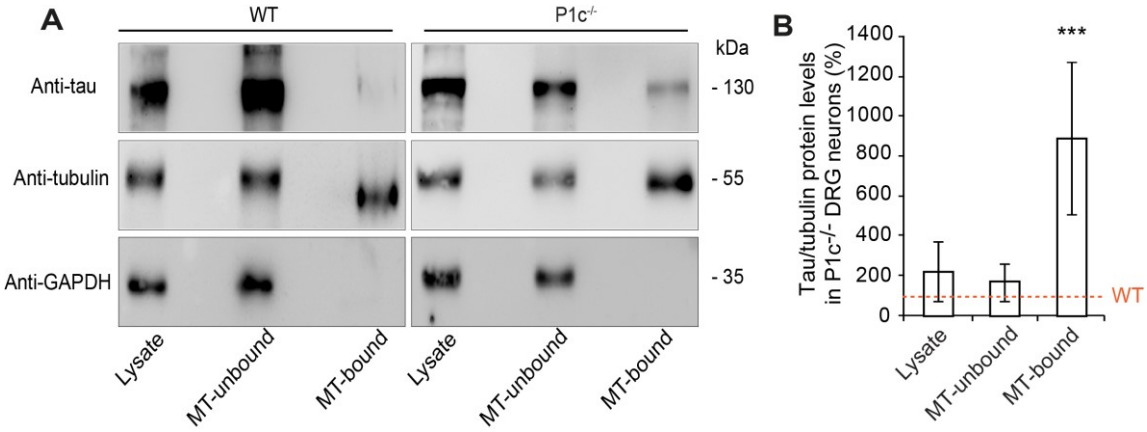

Figure 16.Plectin-dependent association of tau with intact MTs isolated from DRG neurons

A) Cell lysates prepared under MT-stabilizing conditions from WT and P1c-deficient mouse DRG neurons were fractionated, and total cell lysates together with fractions containing MT-unbound, and MT-bound tau were analyzed by immunoblotting using antibodies as indicated. **(B)** Block diagram showing tau signal intensities normalized to tubulin levels. Mean ± SEM (n=3). P-values ***<0.001

To extend my studies to neurons derived from the CNS, I isolated hippocampal neurons and subjected them to similar analyses. Immunofluorescence microscopy of hippocampal neurons using antibodies to tau and tubulin again revealed that in the absence of plectin more tau was bound to MTs than in WT cells (Fig. 17A).

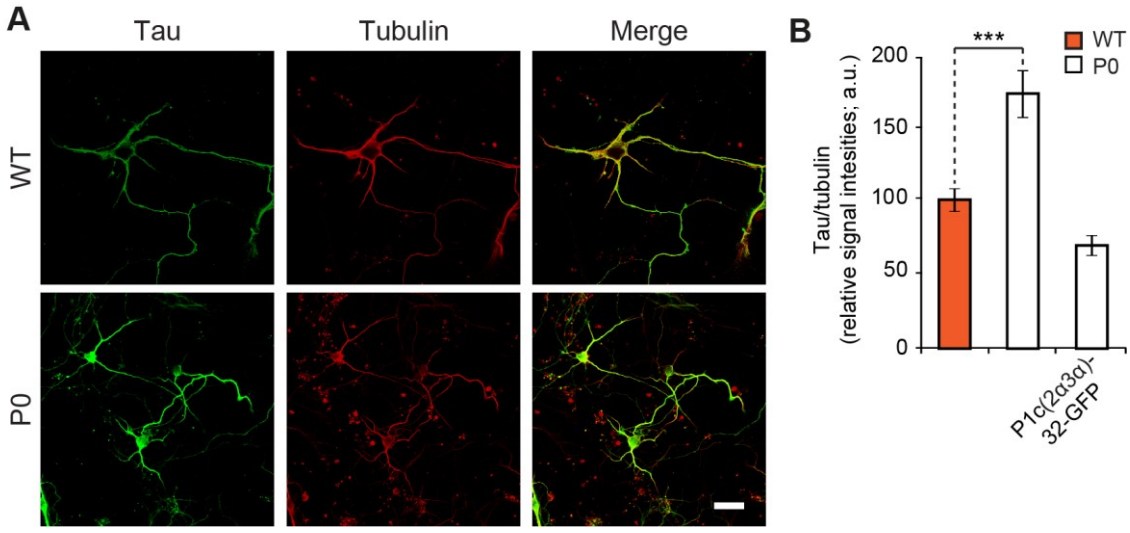

Figure 17. Restoration of low levels of MT-bound tau in plectin-deficient hippocampal cells through expression of full-length P1c

(**A)** Immunofluorescence microscopy of WT and P0 hippocampal neurons double-labeled for tau and tubulin. Scale bar, 20 µm. **(B)** Bar graph shows tau-specific signal intensities (normalized to tubulin levels) measured in untransfected WT, untransfected P0, and full-length P1c-transfected P0 hippocampal neurons (all signals were recorded below saturation levels). Mean ± SEM (axons analyzed: WT n=25; P0 n=14; P0+P1c(2α3α)-32-GFP n=23). Note the 1.74-fold increased tau to tubulin ratio in P0 cells. The transfection of P0 cells with full-length P1c restored their tau signal levels to that of WT controls. P-values ***<0.001

A semi-quantitative statistical analysis confirmed these observations, showing that in the absence of plectin the tau to tubulin ratio was increased to ~174% of the WT level (Fig. 17B). Additionally, conducting rescue experiments where P0 neurons were transfected with an expression plasmid encoding GFP-tagged full length P1c (P1c(2α3α)-32-GFP), the amount of MT-bound tau was reduced to a level even below that of WT cells (~69%) (Fig. 17B).

MTs of P1c-deficient neurons exhibit elevated levels of acetylated α-tubulin

Previous studies showed that posttranslational modifications, especially acetylation of α-tubulin, are important indicators for increased MT stability (Bulinski, Richards, and Piperno 1988; Gundersen 1989), by softening the filaments and making them more resistant against mechanical bending (Janke and Montagnac 2017; Portran et al. 2017). Together with the finding that tau association with the labile domains of MTs make them more dynamic (Qiang et al. 2018) and my own previous results that in P1c$^{-/-}$ neurons tau association is increased with MTs, I wanted to assess whether this was also reflected by the MTs being more extensively acetylated.

In a first approach, DRG neurons isolated from WT and P1c$^{-/-}$ mice were subjected to double immunolabeling using specific antibodies to acetylated α-tubulin and antibodies to α-tubulin that recognized both, acetylated and non-acetylated α-tubulin. Indeed, in P1c-deficient neurons the intensity of the signal specific for acetylated tubulin appeared higher than in the WT cells, whereas the signal for total tubulin (not discriminating between acetylated and non-acetylated species) visually did not show a significant difference (Fig. 18A). Measuring pixel

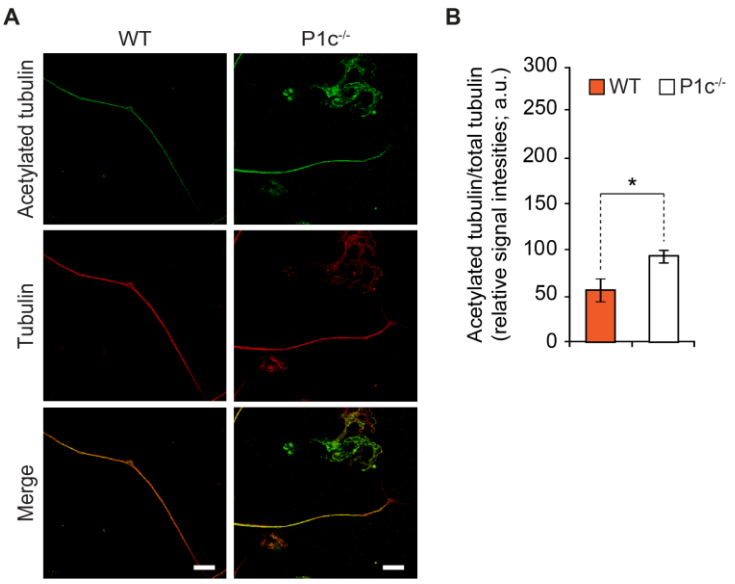

Figure 18. Relative proportions of acetylated to total tubulin in WT and P1c$^{-/-}$ DRG neurons assessed by immunofluorescence microscopy (legend on page 49, bottom)

intensities, a nearly 2-fold increase of acetylated α-tubulin was observed in P1c-deficient neurons compared to WT cells (Fig. 18B).

To establish a direct link between P1c deficiency and increased MT acetylation, rescue experiments were performed. For this, P1c$^{-/-}$ neurons were transiently transfected with expression plasmids encoding either truncated versions of P1c (P1c-30-GFP or P1c-8-GFP) or full-length P1c (P1c-32-GFP) and subsequently the extent of acetylation was determined by immunofluorescence microscopy. Determining the ratio of acetylated to total tubulin for each case, only full-length plectin was found to be fully rescue-competent, lowering the tubulin acetylation level to nearly WT levels (Fig. 19). Expression of the truncated version

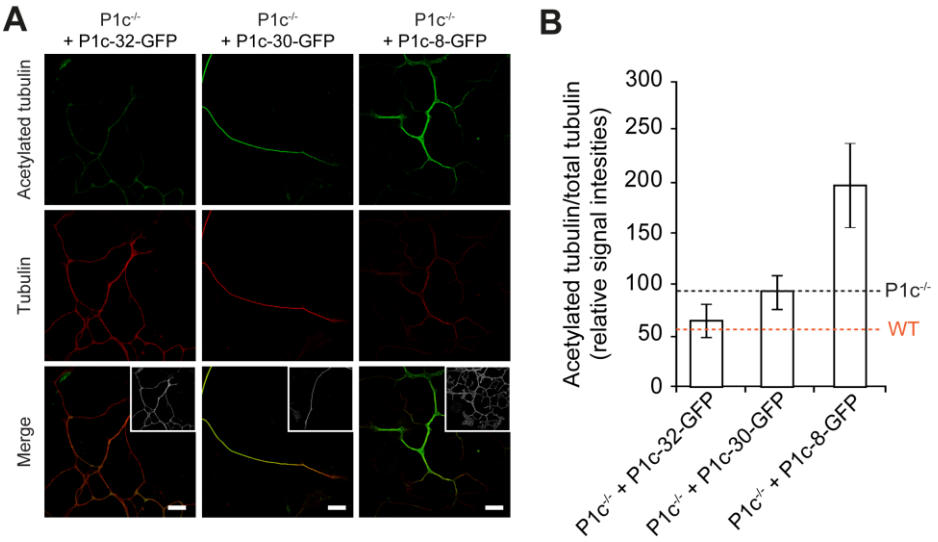

Figure 19. Relative proportions of acetylated to total tubulin in transfected P1c$^{-/-}$ DRG neurons assessed by immunofluorescence microscopy

A) For double immunolabeling antibodies specific to acetylated (green) and anti-tubulin antibodies not discriminating between acetylated and non-acetylated tubulin (red) were used. Scale bars, 4 µm. **(B)** For statistical evaluation signal intensities of acetylated tubulin were normalized to total tubulin. Mean ± SEM (axons analyzed: P1c$^{-/-}$ + P1c-32-GFP n=30; P1c$^{-/-}$ + P1c-30-GFP n=18; P1c$^{-/-}$ + P1c-8-GFP n=20)

Legend to Figure 18: Relative proportions of acetylated to total tubulin in WT and P1c$^{-/-}$ DRG neurons assessed by immunofluorescence microscopy

A) For double immunolabeling antibodies specific to acetylated (green) and anti-tubulin antibodies not discriminating between acetylated and non-acetylated tubulin (red) were used. Note, P1c$^{-/-}$ DRG neurons are strongly immunoreactive with antibodies to acetylated tubulin, contrary to WT cells. Scale bars, 4 µm. **(B)** For statistical evaluation signal intensities of acetylated tubulin were normalized to total tubulin. Mean ± SEM (axons analyzed: WT n=23; P1c$^{-/-}$ n=19). P-values *<0.05

P1c-30-GFP had no effect, as the level of acetylation was equivalent to that of P1c$^{-/-}$ cells, while expression of P1c-8-GFP unexpectedly led to a dramatic increase of acetylation (3.2-fold over WT and 2-fold over P1c-deficient neurons). These results showed that P1c has an important impact on MT acetylation probably affecting MT stability.

To investigate whether the levels of acetylated tubulin were increased also in plectin-deficient neurons derived from CNS, hippocampal neurons were isolated from newborn WT and P0 mice and immunolabeled for acetylated tubulin and total α-tubulin. Similar to DRG neurons, immunofluorescence images revealed stronger signals for acetylated tubulin in P0 compared to WT neurons (Fig. 20A). Quantitative estimates showed that in P0 neurons more than twice as much acetylated tubulin was present compared to WT cells (Fig. 20B).

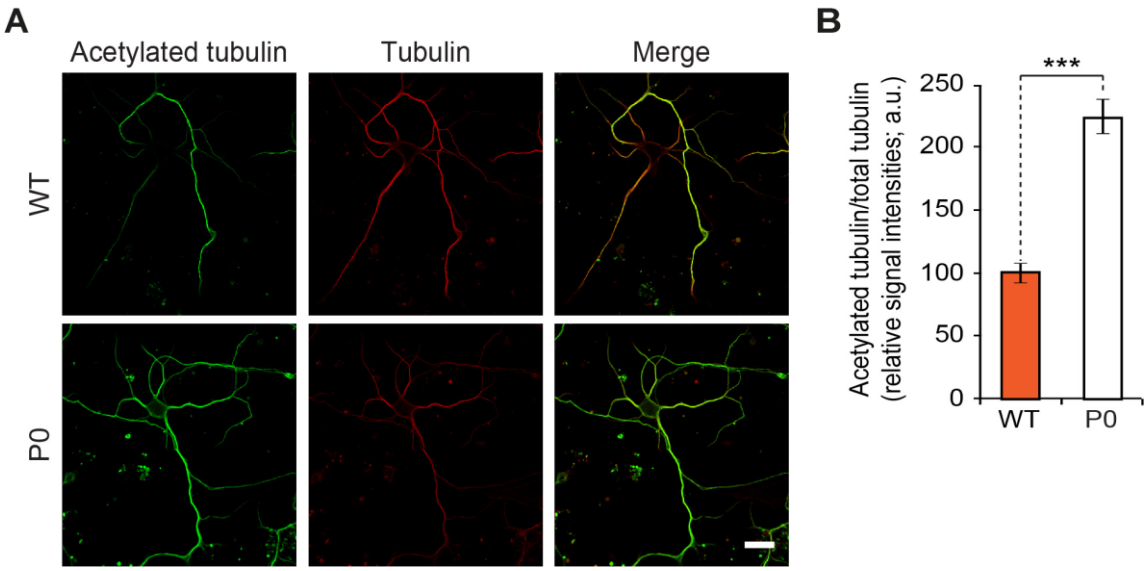

Figure 20. Relative proportions of acetylated to total tubulin in WT and plectin-deficient (P0) hippocampal neurons assessed by immunofluorescence microscopy

A) For double immunolabeling antibodies specific to acetylated (green) and anti-tubulin antibodies not discriminating between acetylated and non-acetylated tubulin (red) were used. Scale bars, 4 µm. **(B)** For statistical evaluation signal intensities of acetylated tubulin were normalized to total tubulin. Mean ± SEM (axons analyzed: WT n=35; P0 n=34). P-values ***<0.001

Elevated levels of acetylated tubulin could be found also on intact MTs isolated from brain lysates of P1c KO mice using high-speed centrifugation under MT-stabilizing conditions. In this case immunoblotting using antibodies specific

for acetylated tubulin and antibodies not discriminating between acetylated and non-acetylated tubulin confirmed that ~1.6 times more acetylated tubulin was found in total cell lysates of P1c$^{-/-}$ compared to WT cells (Fig. 21). In the corresponding MT-unbound fraction a decrease of acetylated tubulin (down to ~40%) was observed, while similar ratios were measured for the MT-bound fraction (Fig. 21). The data obtained by immunolabeling and fractionation combined provided strong evidence that P1c deficiency leads to an elevation of acetylated tubulin levels on stable axonal MT domains in neurons of the PNS as well as the CNS.

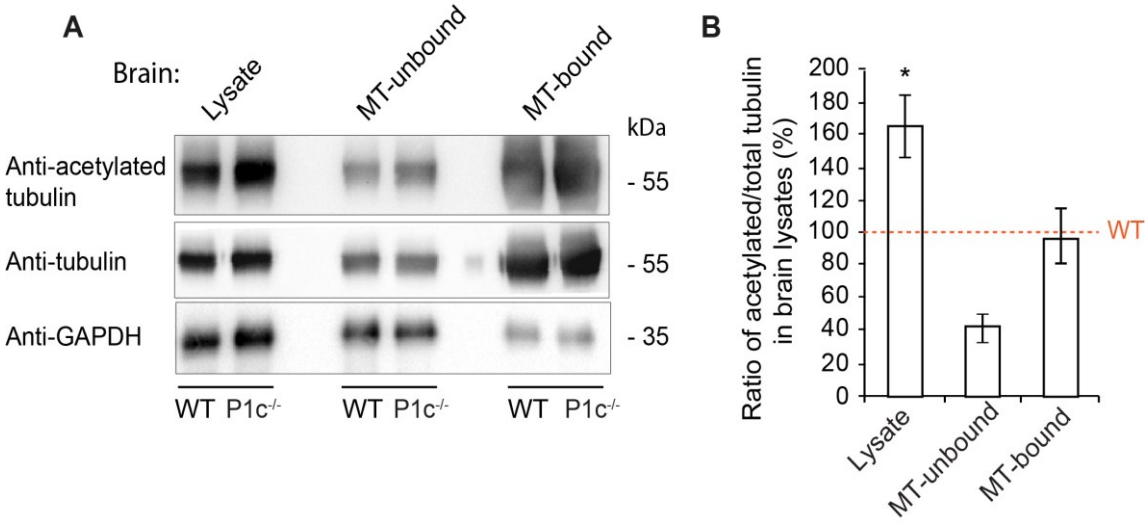

Figure 21. Acetylated tubulin levels in total and fractionated brain lysates

A) Cell lysates prepared under MT-stabilizing conditions from WT and P1c-deficient mouse brain were fractionated, and total cell lysates together with fractions containing MT-unbound, and MT-bound lysates were analyzed by immunoblotting using antibodies as indicated. **(B)** Block diagram showing acetylated tubulin signal intensities normalized to total tubulin levels. Mean ± SEM (n=3). P-values ***<0.05

P1c acts as a regulator of neuritogenesis and growth cone morphology

During development neurons undergo morphological changes, including neuritogenesis, neurite outgrowth and neurite branching, all of which require a dynamic MT network. MTs must interact with various MT-interacting proteins to regulate their dynamic state. The observations described above suggested that P1c not only co-localizes with MTs but also affects their dynamics. During

neuritogenesis the establishment of bundled MTs of uniform polarity is essential to determine axon formation (Witte, Neukirchen, and Bradke 2008; reviewed by Conde and Cáceres 2009). The more stable MTs are, the better it is for axon formation, while dendrites contain usually short and dynamic MTs (Witte, Neukirchen, and Bradke 2008). Thus, in this thesis I wanted to assess whether P1c contributes to physiological characteristics of neuronal cells by comparatively examining neuritogenesis and branching in P1c-deficient and WT neurons.

To monitor neurite outgrowth, DRG explants derived from WT and P1c$^{-/-}$ mice were cultured on matrigel covered with DRG growth medium for 72 h. Fig. 22A shows phase contrast images of cells after 1, 2, and 3 days of culture.

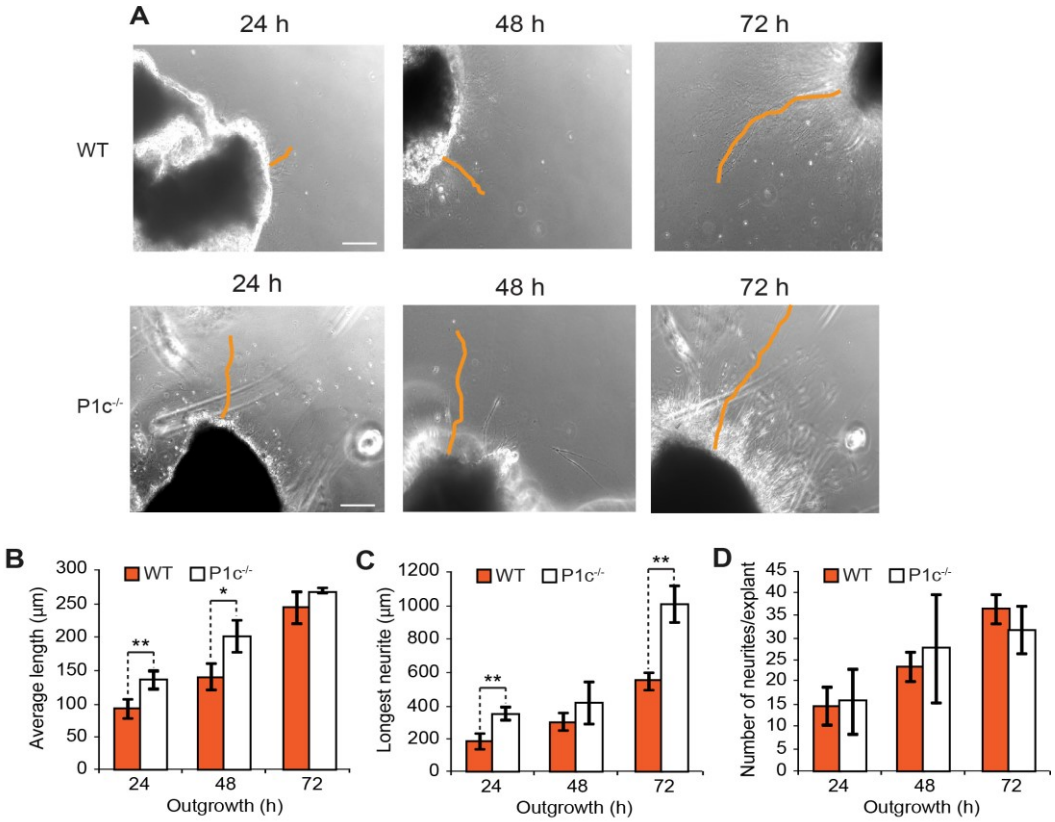

Figure 22. P1c affects neuritogenesis

A) DRG explants derived from WT (upper row) and P1c$^{-/-}$ (lower row) mice were cultivated in matrigel and representative phase contrast images of the outgrowing neurites were taken after plating at time points indicated. Orange outlinings, longest neurite visualized. Scale bar, 100 µm. **(B-D)** Statistical evaluation of average neurite length (B), length of longest neurite (C), and total number of outgrowing neurites (D), all per explant. Mean ± SEM (explants analyzed: WT n=59; P1c$^{-/-}$ n=61) P-values *<0.05, **<0,01

It turned out that at the 24 h and 48 h time points neurites in P1c$^{-/-}$ DRG explants on average were significantly longer than those in WT explants (Fig. 22B); at the 72 h time point the average length was still increased, but the difference was not significant anymore, probably because many DRG explants started to float off at this time point and could not be recorded any longer. Monitoring the longest neurite at the 72 h time point it reached a length of ~1000 µm, while the longest WT neurite grew up to only 500 µm (Fig. 22C). Finally, when the number of neurites per explant was determined, no significant differences between WT and P1c-deficient explants could be detected at any time point (Fig. 22D). To sum up, in the absence of P1c the neurites seemed to become more resistant against depolymerization and therefore were growing faster and became longer.

In a second approach, neurites of P1c-deficient DRG neurons were subjected to a similar analysis. In this case neurites were visualized by labeling their actin cytoskeleton with Texas-Red-coupled phalloidin. Similar to the DRG explants, P1c$^{-/-}$ DRG neurons in culture showed a significant increase in average neurite length (up to 233 µm) compared to their WT counterparts (158 µm) (Fig. 23A); the longest neurites measured were 337 µm and 284 µm for P1c$^{-/-}$ and WT neurons, respectively (Fig. 23B). After transient transfection of P1c$^{-/-}$ cells with

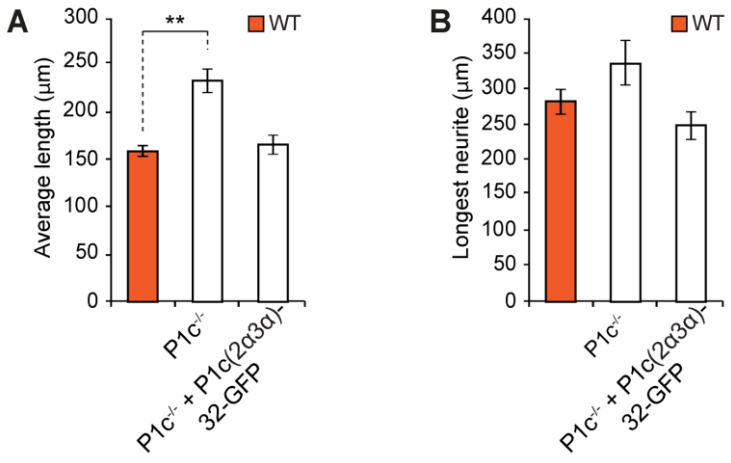

Figure 23. P1c deficiency affects neuritogenesis in cultured DRG neurons

Statistical evaluation of average length **(A)**, and length of longest neurite **(B)** of transfected and untransfected DRG neurons are shown. Mean ± SEM (axons analyzed: WT n=155; P1c$^{-/-}$ n=102; P1c$^{-/-}$ + P1c-(2α3α)-32-GFP n=37). P-values **<0,01

full-length P1c-(2α3α)-32-GFP neurites showed a decrease in average neurite length (from 233 μm to 165 μm) reaching a value similar to that of WT cells (158 μm) (Fig. 23A). Moreover, the longest neurite in transfected cells extended only over 249 μm dropping in length even below the value (284 μm) of the WT control cells (Fig. 23B).

Aside from neurite outgrowth, it was of interest to examine possible effects of P1c deficiency on axonal branching, which plays a crucial role in neuronal development and functionality. Based on my previous results which suggested that P1c-deficient cells contain more stable MTs and form longer neurites, I hypothesized that their axonal protrusions probably would be less branched than those of their WT counterparts. For statistical evaluation, WT, P1c$^{-/-}$, and P1c-(2α3α)-32-GFP transfected DRG neurons were fluorescently labeled (Texas-Red-coupled phalloidin) to visualize the cellular protrusions (Fig. 24A).

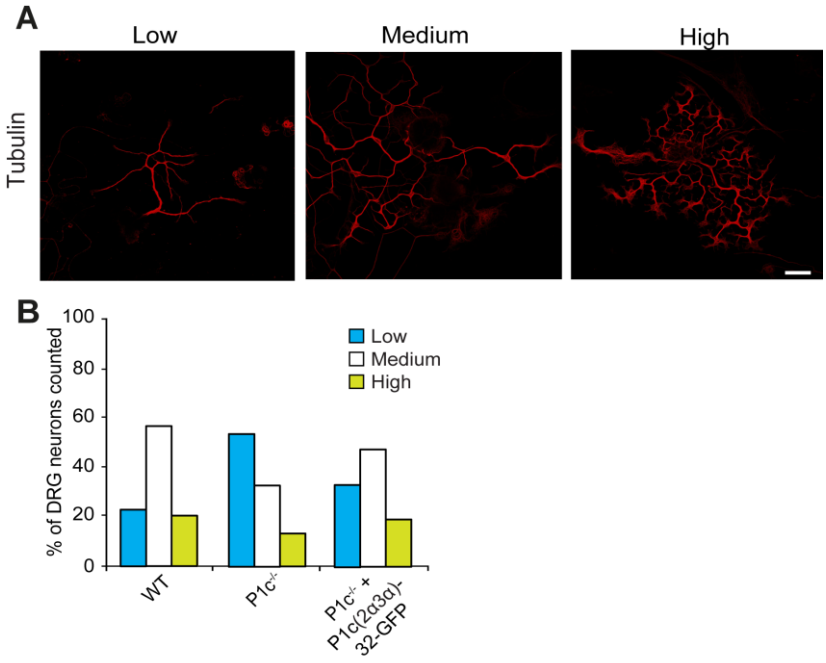

Figure 24. P1c-deficiency affects axonal branching of DRG neurons

(A) Typical examples of fluorescently labeled DRG neurons classified into 3 categories specified in the text (low, medium and high branching per neurite length). Scale bar, 20 μm. **(B)** Statistical evaluation of branching points identified in untransfected WT and P1c$^{-/-}$ DRG neurons, and in P1c$^{-/-}$ DRG neurons transfected with an expression plasmid encoding GFP-tagged full-length P1c (P1c(2α3α)-32-GFP). Neurites analyzed: WT n=132; P1c$^{-/-}$ n=108; P1c$^{-/-}$ +(P1c(2α3α)-32-GFP) n=27. Note the shift from low to medium and high-level branching in transfected cells

Using ImageJ software, the number of manually tracked branching points per neurite length was determined and neurons were classified. Neurons with <1.5, 1.5-3, or >3 branching points were classified as low, medium, and high branching, respectively, with examples being shown in Fig. 24A. Comparing WT and P1c$^{-/-}$ neurons according to this classification, the majority (57%) of WT neurons showed medium branching, while only 33% of P1c$^{-/-}$ neurons fell into this category, and most of the rest (54% of the total) showed low branching (Fig. 24B). In both cases the number of highly branched neurons was comparatively low (WT: 20%; P1c$^{-/-}$: 13%). In a rescue experiment with full-length P1c (P1c(2α3α)-32-GFP) restoration of control values could be reached. Upon transfection, the level of low-branching neurons was down to 33% and the number of highly branched neurons up to 19%, very similar to the WT control. Lastly, the number of medium-branched neurons increased from 33% to 48% (Fig. 24B).

In addition to DRG neurons, hippocampal neurons were subjected to a similar analysis (Fig. 25A and B).

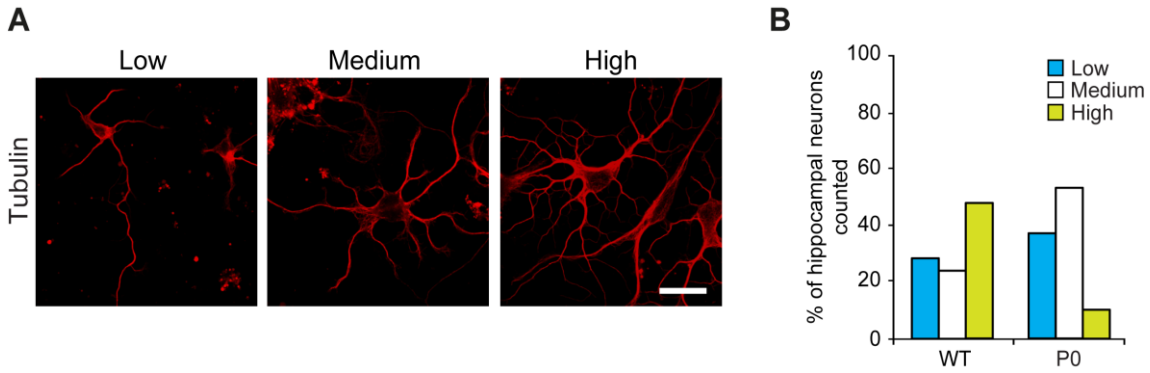

Figure 25. Plectin defciency affects axonal branching of hippocampal neurons

(A) Typical examples of fluorescently labeled hippocampal neurons classified into 3 categories specified in the text (low, medium, and high branching per neurite length). Scale bar, 20 µm. (B) Statistical evaluation of branching points identified in WT and P0 hippocampal neurons. Neurites analyzed: WT n=34; P0 n=28

In this case the three categories of low, medium, and high branching were defined as neurons having less than 2, between 2 and 4, and more than 4 branching points per neurite length, respectively. Similar to DRG neurons, plectin-deficient (P0) hippocampal neurons showed more frequently low branching (37%) compared to WT neurons (28%), and again only a few cells (11%) were highly branched (Fig. 25B). Interestingly, in this case more than half of the P0 cells (52%)

showed medium branching, while only 24% of WT cells fell into this category. Furthermore, nearly half of the WT hippocampal neurons (48%) were classified as highly branched (Fig. 25B). Taken together, the analysis of DRG and hippocampal neurons revealed that, compared to plectin-deficient neurons, WT cells have more branches along their neurites and not more than a fourth of them show low branching.

As a next step I investigated whether plectin deficiency affects growth cone morphology. As the MT as well as the actin cytoskeleton network systems both play an important role in growth cone formation and both systems have been shown to be affected by plectin deficiency, a growth cone phenotype was to be expected. Indeed, when I measured growth cone areas and growth cone perimeters of Texas-Red-coupled phalloidin stained WT and P1c-deficient neurons (Fig. 26), the latter showed significant increases in both parameters compared to their WT counterparts. Growth cones of P1c-deficient DRG neurons were ~1.5 times longer and their perimeters were ~1.3-fold increased (Fig. 26B and C). It was mainly the multitude of protrusions distributed along the surface of the P1c-deficient growth cones (Fig. 26A) that contributed to the increased perimeter. While in WT cells most protrusions were concentrated and located near the tip of the growth cone, in P1c$^{-/-}$ cells protrusions could be found all around the growth cone (Fig. 26A).

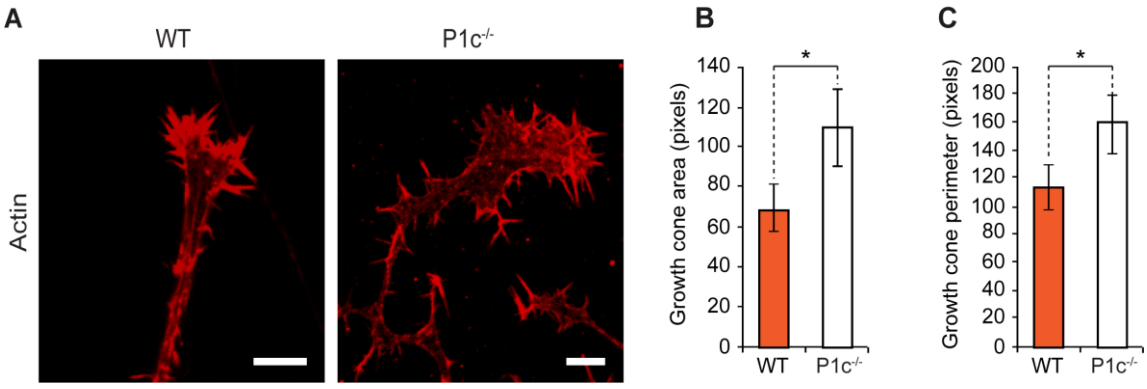

Figure 26. P1c deficiency affects the growth cone morphology of DRG neurons

(A) growth cones of WT and P1c$^{-/-}$ DRG neurons were visualized by labeling cytoskeletal actin with fluorescent phalloidin. Scale bar, 5 µm. **(B,C)** Statistical evaluation of growth cone areas **(B)** and growth cone perimeters **(C).** Mean ± SEM (growth cones analyzed: WT n=21, P1c$^{-/-}$ n=18). P-values *<0.05

Analyzing growth cones of WT and plectin-deficient (P0) hippocampal neurons in a similar way, I found a ~1,8-fold increase in the growth cone area of P0 compared to that of WT hippocampal neurons (Fig. 27B). Additionally, ~1,5 times more protrusions were visible in P0 hippocampal neurons. Furthermore, the growth cone perimeter of KO cells was increased by a factor of ~1,6 fold (Fig. 27C).

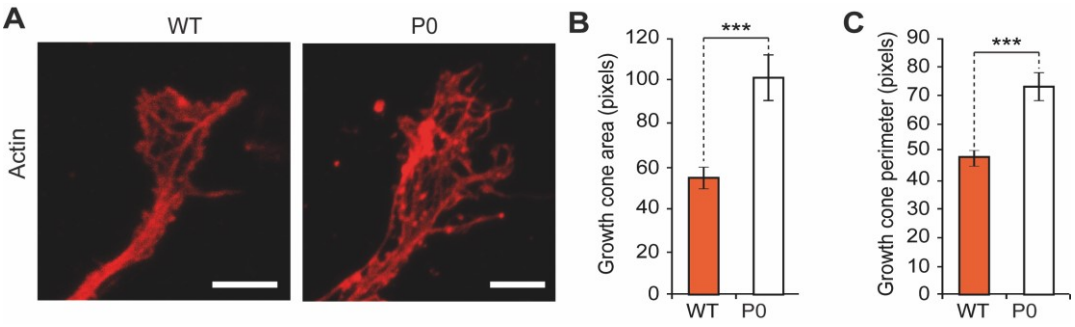

Figure 27. P1c deficiency affects growth cone morphology of hippocampal neurons

(A) growth cones of WT and plectin-deficient (P0) hippocampal neurons were visualized by labeling cytoskeletal actin with fluorescent phalloidin. Scale bar, 5 µm. **(B,C)** Statistical evaluation of growth cone areas **(B)** and growth cone perimeters **(C).** Mean ± SEM (growth cones analyzed: WT n=30, P1c$^{-/-}$ n=30) P-value ***<0.001

Discussion

Plectin 1c interacts isoform-specifically with neuronal MTs

Using immunofluorescence microscopy, I was able to show in this study that P1c associates with MTs along the neurite shaft and in the growth cone of neuronal cells. Moreover, I found that P1c´s interaction with MTs was isoform-specific, as colocalization with MTs was observed after transfection of neurons with cDNA expression plasmids encoding a full-length version of P1c (P1c(2α3α)-32-GFP), or a truncated version (P1c(2α3α)-8-GFP), but not when corresponding versions of isoform P1f were expressed. These findings correlated with similar observations made earlier in studies with keratinocytes. Valencia et al. (2013) reported that in keratinocytes P1c colocalizes with MTs in a dotted pattern, leading to alterations in MT network organization when absent. However, in contrast to keratinocytes, in neurons, I found P1c to decorate MTs not in a dotted pattern but rather evenly distributed all along the MTs surface at high density. This suggests that the major isoform of plectin expressed in neurons, P1c, is predominantly associated with MTs.

Antagonizing tau-MT association, P1c plays a role in MT dynamics

The levels of acetylated α-tubulin in DRG as well as in hippocampal neurons were increased in P1c-deficient compared to WT mice. This was demonstrated using two different assays, co-localization with cytoplasmic MTs and co-sedimentation with MTs after cell fractionation. For P1c-deficient DRG as well as hippocampal neurons, I could record an approximately 100% increase in MT acetylation using antibodies specifically recognizing the acetylated form of α-tubulin. In addition, I found that brain lysates derived from P1c-deficient mice contained 1.6 times more acetylated tubulin than WT lysates, whereby nearly all of the tubulin incorporated into polymers, was acetylated. Moreover, forcing the expression of full-length P1c in P1c-deficient DRG neurons, a nearly complete restoration of WT levels of tubulin acetylation was observed, demonstrating that

in the presence of P1c less tubulin modifications occurred, probably allowing MTs to be more dynamic. Interestingly, rescue attempts with truncated versions of P1c, lacking the rod and C-terminal IF-binding domains, were unsuccessful, and in the case of P1c-8-GFP, there was even an increase in acetylation of up to over 300% compared to WT neurons. Recent studies on MT stability revealed that MTs comprise labile and stable domains where labile domains contain less acetylated tubulin, favoring MT dynamics (reviewed by Baas et al. 2016). My results clearly showed that in the absence of intact P1c, MTs show a higher degree of acetylation, indicative of higher stability (Bulinski, Richards, and Piperno 1988). Furthermore, in previous studies R. Valencia (PhD thesis 2012) showed MTs in DRG neurons to be more resistant towards nocodazole-induced disassembly in the absence of P1c, which was consistent with the hypothesis that P1c plays a role in MT dynamics through its MT destabilizing function.

Hammond et al (2010) reported that secondary protein modifications such as acetylation have a strong influence on transport events along MTs and their binding to MAPs. Furthermore, a mechanistic model exists where P1c is targeted directly to the surface of axonal MTs via its isoform-specific N-terminal sequence, while P1c´s SH3 domain (located further downstream) interferes with the binding of MTs to tau protein. Recent studies on MAP-MT interaction revealed that tau proteins preferentially are associate with the labile domains of MTs, allowing MTs to have longer dynamic areas (Qiang et al. 2018). This is consistent with my own results, showing that P1c as a MAP antagonist acts as a MT destabilizer. My own observations regarding the functional role of P1c as MAP antagonist, which were based on co-sedimentation and co-localization assays indeed revealed more tau bound to MTs in P1c$^{-/-}$ compared to WT neurons. This was true for DRG neurons, hippocampal neurons as well as whole mouse brain lysates. In all of these cases a nearly 2-times higher level of MT-bound tau could be measured in the absence of P1c, while in WT samples more unbound tau was detectable. Importantly, by forced expression of full-length P1c and two N-terminal plectin fragments (P16-24 and P20-21-GFP) in DRG neurons a reduction of MT-bound tau levels could be achieved, whereby P1c-20-21-GFP turned out to be most effective. This confirmed previous results suggesting that plectin´s SH3 domain has the capacity to interact with MAPs, including tau, thereby interfering with their MT regulatory

function. My results were thus consistent with previous studies on the role of P1c in keratinocytes (Valencia et al. 2013).

Based on these results one may speculate that plectin has an influence on neuronal mechanisms that are important for proper nerve cell functions such as axonal transport. Recent single-molecule studies revealed a short interaction time of tau with MTs (less than 40 ms), called “kiss and hop” mechanism (Janning et al. 2014). This explains why tau normally does not interfere with axonal transport, even though the binding sites of tau and the axonal motor proteins kinesin and dynein are lying along the same path along the MT surface (Dixit et al. 2008). In this context, I would like to propose that due to the absence of plectin, the interaction of tau and MTs is likely to be too strong to maintain the “kiss and hop” mechanism, which in turn leads to increased tau-binding and interference with motor proteins, with consequences for the axonal transport, such as that of NFs (see below).

The outcome of my study may also be of relevance for neurogenerative disorders such as tauopathies. The best known tauopathy is Alzheimer´s disease, manifesting with tau aggregation and increased tubulin acetylation (Perez et al. 2009). MT-bound tau has been reported to act as an inhibitor of histone-deacetylase-6 (HDAC6), thereby suppressing HDAC6´s ability to deacetylate tubulin polymers and consequently leading to increased levels of acetylated α-tubulin. Having in mind that tubulin acetylation is not a cause of MT stabilization, but rather its consequence (reviewed by Creppe et al. 2009), it would be interesting to compare the molecular mechanism and pathological symptoms associated with neurons from Alzheimer´s disease patients with those from P1c$^{-/-}$ mice. Both types of neurons exhibit high levels of acetylated tubulin, but one manifests with tau aggregation, while the other with accumulation of tau on MTs.

NF network organization and dynamics are plectin-dependent

Compared to WT, I found NFs in the growth cone area of P1c$^{-/-}$ DRG neurons to have a fan-like organization, often being less bundled, more dispersed, and extending deeper into the growth cone interior. In contrast, WT controls displayed highly condensed NFs with a ring-like structure anchored in the axon-growth cone transition area, while very few such structures were found

in plectin-deficient neurons. These observations were consistent with phenotypic alterations of IFs expressed in other types of cells. E.g., vimentin filaments in plectin-deficient fibroblasts are dispersed and unorganized particularly at the cell periphery (Burgstaller et al. 2010; Gregor et al. 2014). On this basis and with the knowledge that plectin interlinks IFs with various cellular structures and organelles, including transmembrane junctional complexes, the nuclear envelope, mitochondria and others, and mediates their crosstalk with the actin and MT cytoskeleton networks, one can assume similar crosslinking mechanisms to be underlying NF functions in neurons. I propose that P1c keeps NFs in a rather compact state, anchoring them at the neck of the growth cone, thereby preventing their uncontrolled penetration into the highly dynamic growth cone area. My results provided evidence for this hypothesis, as they showed that NF organization in P1c$^{-/-}$ DRG neurons was altered, as less bundled filaments protruding into growth cones were observed. However, phenotype manifestation was not tight, i.e. a few P1c KO neurons were found that still exhibited the ring-like structure characteristics of WT cells, while occasionally WT neurons were encountered where NFs were intruding into the growth cone without assuming a ring-like shape, even if the penetration depth was considerably less than in P1c$^{-/-}$ DRG neurons. The generated results cannot yet explain the molecular mechanisms how the anchorage of NFs at the transition area comes about. In particular it will be of great interest to investigate the role of the focal adhesion proteins paxillin, vinculin, talin, and integrins in NF-anchoring, as proteins of this type are already known from studies with fibroblasts to mediate IF-actin crosstalk by interlinking vimentin with integrins (Burgstaller et al. 2010). In this scenario it is likely that in P1c-deficient cells, the crosstalk between focal adhesion proteins with cytoskeletal networks is disturbed, leading to uncoordinated cytoskeleton arrangements at the axon-growth cone transition area.

Investigating NF transport by FRAP, my analysis revealed that in the absence of P1c NF particles not only moved slower along the axon, but also displayed longer pausing times. No significant difference in movement directionality was found, confirming earlier studies on the bidirectional transport of NFs along axons (Glass and Griffin 1994; Brown, Wang, and Jung 2005). Furthermore, the analyzed NF particles were transported at a slower migration rate in P1c$^{-/-}$ compared to WT neurons and exhibited more often prolonged

pausing times. NFs are usually transported along the neuronal axon via motor proteins (kinesin and dynein) following a stop- and go rhythm of slow axonal transport and thus can be found bound to MTs and moving along them, or disengaged from the MTs in an off-track state, leading to long pausing (Brown, Wang, and Jung 2005). In light of my previous observations including increased MT stability through excessive tubulin acetylation and tau decoration on the labile domains of the MTs (see above), I propose that through the absence of P1c and the higher MT-binding rate of tau molecules the motor protein-dependent transport is impaired, leading to NF particles being more often in an off-track state rather than moving along the axon.

Evaluating signal intensity levels in growth cone areas, I found that in P1c$^{-/-}$ DRG neurons NFs formed loosely packed bundles with drastically reduced signal intensity values compared to the intensively labeled, dense NF rings observed in WT cells. These observations again confirm the hypothesis that, through the tight binding of tau, less NFs are bound to and transported along MTs. On the other hand, it is hard to reconcile the results of slow axonal transport, deep penetration depth and low signal intensities of NFs in P1c$^{-/-}$ neurons. One possibility could be that some NF particles are transported faster than others, but once in the growth cones are not tightly bundled and thus form loose but long filaments. Another possibility would be that in KO cells the retrograde transport of NFs is inhibited and therefore filaments extending into growth cones will not undergo proper disassembly. Further experiments assessing NF stability, post-translational modifications, and NF transport will be needed to better understand the mechanisms underlying NF network alterations arising from plectin deficiency.

P1c plays a role in neuritogenesis

Investigating morphological alterations, I found axonal branching, neurite outgrowth as well as growth cone morphology drastically changed in P1c-deficient DRG as well as hippocampal neurons. Monitoring neurite outgrowth from DRG explants I observed that in P1c-deficient explants the neurites were significantly longer, with the longest one exhibiting double the length of its WT counterpart. Similarly, the average neurite length of DRG neurons was increased in the absence of P1c. Furthermore, transfection of P1c$^{-/-}$ neurons with plasmids

encoding full-length P1c led to phenotype restoration. These results, together with the observed MT-destabilizing function of P1c, confirm the notion that axon formation requires the establishment of stable but still dynamic bundled MTs (Witte, Neukirchen, and Bradke 2008; reviewed by Conde and Cáceres 2009).

Aside from altered neurite formation I found axonal branching to be drastically decreased in P1c-deficient neurons. Moreover, after forced expression of full-length P1c in $P1c^{-/-}$ neurons, branching could be significantly restored in both DRG and hippocampal neurons; in the latter case, even to levels above that of WT cells. These observations suggested that due to the increased stability of MTs in P1c-deficient neurons there existed fewer branching points. Studies of others indicated that MT-associated tau proteins repell MT-severing proteins, such as katanin. In fact MTs having less tau associated with them showed a greater tendency for branching (Yuan et al. 2008). Again, this brings my results in line with P1c being an antagonist of tau-MT interaction.

Having shown that P1c deficiency affects both the MT and the IF network organization in neurons, I expected it to have an effect on the actin cytoskeleton as well. Inspecting growth cone morphology of plectin-deficient neurons, I could show that the areas as well as the perimeters of the growth cones increased dramatically, with similar results for both systems (DRG and hippocampal neurons). Importantly, P1c-deficient growth cones showed actin-rich protrusions all around their perimeters whereas in WT neurons, actin protrusions were mostly found at the tip of the growth cone. As the crosstalk and dynamic coordination between F-actin and MT cytoskeletal networks must work unimpaired for proper performance, my results indicate that this is not the case for $P1c^{-/-}$ neurons. Probably NFs are not anchored correctly to the membrane and/or other network components, leading to an abnormal shape of growth cones due to distortions of the actomyosin filament system. Since an important role of growth cones is to guide the axons to their targets during neuronal development and to navigate the extracellular cues presented (reviewed by Cammarata, Bearce, and Lowery 2016), it will be important to investigate in more detail the mechanisms leading to disruption of cytoskeleton network organization in growth cones of neurons upon suppression of plectin.

Conclusion

This master thesis led to new insights into the role played by plectin isoform P1c in PNS (DRG) and CNS (hippocampal) neurons. The acquired data confirmed that P1c has a MT-destabilizing function competing with tau for MT-binding. In the absence of P1c, neuronal MTs show alterations in posttranslational modifications, in particular increased acetylation of their α-tubulin subunits in their stable domains, which presumably makes them more resistant against mechanical stress and bending. Furthermore, tau proteins become enriched on the labile domains of MTs, thereby promoting MT assembly. The more stable but still dynamic MTs in P1c-deficient neurons lead to altered NF network organization, paralleled by changes in neurite length, changes in growth cone shape and axonal branching. In the future, it will be of interest to address the molecular mechanisms underlying these phenomena. In all, we are just at the beginning of understanding the importance of P1c for the functions of neurons, but the results obtained in this study should be helpful in guiding future research into promising directions.

Materials and Methods

Animals

Animals used for DRG isolation were 8-12 week-old C57BL/6J (WT) and P1c$^{-/-}$ (Plec/Parp$^{10tm1.1Gwi}$) mice. For hippocampal neurons newborn WT and P0 (Plec^{tm1Gwi}) mice were used. All mice were fed ad libitum, housed in a temperature- and humidity-controlled room with a pathogen-free environment and a 12 hour light-dark cycle.

Plasmids and preparation of plasmid DNA

For transfection experiments of mammalian cells the following expression plasmids were used: Full-length mouse P1c and P1c-8 with C-terminal EGFP tags, described previously (Rezniczek et al. 2003; Burgstaller et al. 2010), plectin fragments corresponding to exons 1c-8 (P1c-8, pGR337) and exons 1c-30 (P1c-30, ampGR324), exons 16-24 (P16-24, pGR329), exons 20-21 (P20-21, pGR331), exons 1c-(2α3α)-8 were engineered by Rezniczek (2003) based on published sequences (Fuchs et al. 1999). For protein expression in bacteria, BL21 (DE3)$_{RIL}$ *E. coli* were transformed and bacterial stocks were frozen on -80°C. Plasmid DNA purification from bacteria was carried out with PureYield™ Plasmid Midiprep System kit from Promega. For this, 100 ml of transformed E.coli bacteria were grown overnight at optimal culture conditions and further steps were done according to the manufacturer´s instructions (Promega). Concentrations of the obtained endotoxin-free plasmid DNA were measured using NanoDrop™1000 spectrophotometer from Thermo Fisher Scientific, it enables an accurate analysis of 1 µl samples.

Isolation and cultivation of dorsal root ganglia

Medium and solutions:

<u>poly-L-lysine hydrobromide solution:</u>

1% poly-L-lysine hydrobromide in sterile H_2O (Sigma-Aldrich)

Laminin solution:

	PBS (Gibco®)
1%	laminin (1 mg/ml PBS, Sigma-Aldrich)

Collagenase solution (1 ml/mouse):

200 µl	2% collagenase type 2 (4000 U/ml, Sigma-Aldrich)
20 µl	horse serum (Gibco®)
780 µl	DMEM-F/12 + GlutaMAX (Gibco®)

Trypsin solution (1 ml/mouse):

500 µl	normal trypsin solution
1 µl	DNAse I (Roche)
499 µl	PBS (Gibco®)

Normal trypsin solution:

0.05%	trypsin (Gibco®)
0.2 mg/mol	EDTA
	HBSS (Gibco®)

Stop solution (2 ml/mouse):

1.6 ml	DMEM-F/12 + GlutaMAX (Gibco®)
400 µl	horse serum (Gibco®)

Growth medium (2 ml/mouse):

10 µl	penicillin/streptomycin (5000 U/ml-5000 µg/ml, Gibco®)
100 µl	horse serum (Gibco®)
20 µl	N2-supplement (100x, Gibco®)
1.87 ml	DMEM-F/12 + GlutaMAX (Gibco®)

For cultivation of DRG neurons sterile glas coverslips or ibidi µ-dishes (35 mm, company ibidi) were coated with poly-L-lysin and laminin to enable a good bond between neurons and the glass surface. For immunostaining isolated DRG neurons were plated on coated glass coverslips in 24 well plates, for live microscopy µ-dishes were used as plating material. 300 µl poly-L-lysine (10 µg/ml

ddH_2O) (Sigma-Aldrich, P1524) was added to each coverslip or dish and incubated for 1 h at 37°C, and finally washed 3 times with ddH_2O. The coated coverslips can be stored up to one week in 24 well plates at 4°C in the dark. Before further use, the coverslips and dishes were additionally coated with laminin (10 µg/ml PBS) and incubated for 3 h at 37°C. After incubation, the coverslips were washed 3 times with PBS and 500 µl growth medium was added.

DRG neurons were isolated from adult (8-12 week old) P1c$^{-/-}$, plectin-deficient and WT mice, following the protocol of Stroissnigg et al. (2007). First, the mice were sedated through inhaling the anesthetic gas IsoFluoran (100 µl dropped on tissue paper) inside a closable chamber. The sedated mice were decapitated, and the skin and other tissue were carefully removed from the spine. The backbone of the spine was opened, and the spinal cord was dissected. The DRG neurons were carefully isolated out of the spine, using a precision tweezer (Carl Roth^{TM}) and a curved micro scissor, and finally collected in ice-cold DMEM-F/12 + GlutaMAX medium in a 15 ml centrifugation tube (Eppendorf). After isolating all DRG neurons, the tube was centrifuged for 3 min at 800 rpm, the supernatant was removed carefully with a Pasteur pipette and 1 ml of collagenase solution was added. The DRG neurons were incubated for 1.5 h at 37°C in a CO_2 incubator. The collagenase solution was replaced with 1 ml trypsin-DNase solution and the DRG neurons were incubated again for 10 min at 37°C in a CO_2 incubator. After the trypsinization step, 2 ml STOP solution was added to inactivate the DNase and the cells were triturated with a fire polished Pasteur pipette (2/3 opening size of original Pasteur pipette size) and afterwards a second time with another even smaller fire polished Pasteur pipette (half opening size of original pipette size). To create fire polished pipettes, the opening end of the Pasteur pipette is continuously rotated over a flame of a bunsen burner till the edges become smooth and the opening size gets smaller. The DRG neurons were finally centrifuged again for 5 min at 800 rpm and the supernatant was replaced with 2 ml fresh growth medium. The cell pellet was resuspended carefully and 500 µl cell suspension was added to each coverslip. The 24 well plate with the growing DRG neurons was placed at 37°C for 24 h.

Isolation and cultivation of hippocampal neurons

Medium and solutions:

poly-L-lysine hydrobromide solution:

10%	poly-L-lysine hydrobromide in sterile H_2O (Sigma-Aldrich)

HBSS dissecting solution:

	HBSS (no phenol red, 14025-100 Gibco®)
20%	1 M HEPES (Gibco®)

Plating medium (DMEM-HS):

	DMEM, high glucose, GlutaMAX I™,pyruvate (Gibco®)
10%	horse serum (Gibco®)

Growth medium:

	Neurobasal™ -A Medium (without phenol red, Gibco®)
2%	B27® serum-free supplement (50x) (Gibco®)
1%	L-glutamine (200 mM, Gibco®)

For cultivation of hippocampal neurons sterile glas coverslips or ibidi µ-dishes (35 mm, company ibidi) were coated with poly-L-lysine (100 µg/ml ddH_2O) (Sigma-Aldrich, P1524), by adding 300 µl to each coverslip or dish and incubating them for 1 h at 37°C in a CO_2 incubator, finally they were washed 3 times with ddH_2O and covered with PBS till usage.

Hippocampi were isolated from newborn plectin-deficient (P0) and WT mice following the protocol of Seibenhener and Wooten (2012). As newborn and young mice up to the age of 21 days are resistant against inhalational anesthetic, the newborn mice were decapitated as fast and painless as possible. The skin was removed from the remaining head and the scull was carefully opened with sharp forceps and a surgical scissor, not cutting or destroying the brain. For further dissection, the brain was removed from the opened scull into a 3.5 cm cell culture dish, filled with pre-warmed HBSS media. Next, the brain was cut into its two hemispheres with a scalpel and the cerebellum was removed. The connective tissue, covering the whole brain, was removed carefully and the hemispheres

were turned on the side; lying now on the cortex. The upper nerve tissue (white fluffy tissue) was removed, underneath the hippocampus (curved structure) is lying connected to the cortex. Further on, with curved forceps the hippocampus was isolated by “rolling” it away from the cortex, carefully removing all remaining tissue that is not part of the hippocampus itself. The isolated hippocampi were transferred into a 15 ml centrifugation tube (Eppendorf) filled with pre-warmed HBSS. From this step on all further processes were done under sterile conditions. After collection of all hippocampi, the HBSS was replaced and incubated with 1 ml pre-warmed trypsin-EDTA solution for 10 min at 37°C. Following the trypsinization step, the hippocampi were washed 2 times with about 5 ml pre-warmed HBSS. After washing the hippocampi, the HBSS was replaced with 4 ml pre-warmed plating medium and the hippocampi were triturated with two different sized fire-polished Pasteur pipettes (about 50% and 30% of usually diameter opening size). The single hippocampal neurons were plated in plating medium for 1.5 h at 37°C in a CO_2 incubator, for resting and moving to the bottom, then the medium was carefully changed to B27-supplemented neurobasal medium (growth medium). The neurons were transferred for 24 to 48 h into an incubator (37°C and 5% CO_2) for growing.

Transient transfection of isolated neurons with plasmid DNA

After neuron preparation (see chapters above) and before plating, the neurons were transiently transfected with plasmids, expressing various plectin isoforms, using the Amaxa® Basic Neuron SCN Nucleofector Kit® (Lonza) following the standard protocol from Lonza and Zeitelhofer et al. (2007). First, the nucleofector kit was equilibrated to room temperature and yellow pipette tips were cut (about 5 mm from the tip), to gain bigger openings. For transfection, $2x10^4$ cells were centrifuged at 800 x rpm for 5 min and the supernatant was removed carefully and completely. The remaining cell pellet was resuspended with a yellow cut off tip in 100 µl nucleofector solution. Trying to avoid bubbles was very important in this step. After resuspension, 1,5 µg endotoxin free plasmid DNA was added to the neurons and the tube was flicked gently two to three times, to mix the DNA with the cell suspension. The cells were then carefully transferred, using one of the yellow cut-off tips, into a SCN cuvette (provided in the kit) which was then placed into the Amaxa machine. Starting program 6 (G-013; Neuronal rat

DRG or Neuronal mouse hippocampus). Immediately after transfection, 500 µl DRG growth medium or plating medium (for hippocampal neurons) was added, and the cuvette was placed inside the CO_2 incubator for 10 min. Then, the cells were plated on pre-coated coverslips or pre-coated ibidi dishes and cultivated at 37°C in a humidified atmosphere of 5% CO_2.

Immunostaining of neuronal preparations

Medium and solutions:

10x PBS:

81.8 g	NaCl
2.01 g	KCl
2.04 g	KH_2PO_4

pH 7.5; ddH_2O add 1000 ml

Fixation solution:

	1x PBS
4%	paraformaldehyde (Sigma-Aldrich)
11%	sucrose (Sigma-Aldrich)

Blocking solution:

	1x PBS
5%	BSA (Sigma-Aldrich)
0.15%	Triton™X-100 (Sigma-Aldrich)

Mowiol mounting medium:

12 g	glycerol
4.8 g	Mowiol 4-88 (Sigma-Aldrich)
24 ml	0.2 M tris-HCl (pH 8.5)
12 ml	ddH_2O

The cultured and transfected neurons (see chapters above) were washed once gently with 1x PBS, by removing the growth medium and adding 500 µl PBS

carefully to the cells. After washing, the PBS was replaced with 500 µl fixation solution and the neurons were incubated for 30 minutes at 37°C. Finally, the neurons were washed again two times after fixation with 500 µl PBS. For the staining, a “wet-chamber” was assembled to prevent the staining solutions to dry out during incubation steps. To cover the whole coverslips with a small amount of solution, the solution itself was dropped on a parafilm (Sigma-Aldrich) and the coverslip was turned upside down, allowing the cells to lie on top of the drop. The coverslips were first blocked for 1 h with 100 µl blocking solution. The coverslips were then washed shortly in 1x PBS and then the primary antibodies, diluted in blocking solution, were added to the wet-chamber and the neurons were placed again on top of the primary antibodies incubating for 3 hours at room temperature. After the first incubation, the cells were washed 3 times for 5 min in fresh 1x PBS and the secondary antibody, diluted in blocking solution, was added to the cells, incubating for 2 hours. The cells were washed again 3 times with fresh 1x PBS for 5 min and finally the coverslips were mounted in 15 µl mowiol mounting medium (high quality anti-fade medium) onto microscope slides.

Confocal microscopy

Microscopy was performed at room temperature using a confocal microscope (Zeiss, LSM 700) equipped with a Plan-Apochromat 63x 1.4 NA or 100x 1.4 NA objective lens. Images were recorded using the LSM 700 module and the Zeiss ZEN software.

Preparation of DRG explants

DRG growth medium:

10 µl	penicillin/streptomycin (5000 U/ml-5000 µg/ml, Gibco®)
100 µl	horse serum (Gibco®)
20 µl	N2-supplement (100x, Gibco®)
1.87 ml	DMEM-F/12 + GlutaMAX (Gibco®)

DRG neurons were dissected from adult mice and harvested in ice-cold DMEM medium and further embedded in a 15 µl Matrigel TM (BD Biosciences)

drop on uncoated coverslips in a 6 well plate and covered finally with 1 ml DRG growth medium. The explants were cultured at 37°C in an CO_2 incubator for 24 h up to 72 h. After every 24 h, images of the DRG neurites were made, using an AxioObserver Z1 microscope coupled to AxioCam MRm (Zeiss) equipped with 32x phase contrast objective at 37°C and 5% CO_2. The taken images were analyzed with ImageJ software to track neurite number/explant, neurite length and longest neurite for every 24 h circle.

Fluorescence recovery after photobleaching

DRG neurons were isolated and transfected with cDNAs expressing GFP-tagged NF-M. The cells were cultured on ibidi-dishes and observed after 24 h with a Zeiss LSM 710 confocal microscope, supplied with a heated stage (37°C) and constant 5% CO_2 flow, using a Plan-Apochromat 63x1.4 NA objective lens with an excitation wavelength of 488 nm. Axonal areas of the neurons therefore were bleached according to using Zeiss ZEN software and the moving NF particles were scanned in intervals of 4 seconds up to 10 minutes.

MT binding assay

Buffers:

Extraction Buffer (4 ml):

640 µl	0.5 M MES
4 µl	1 M $MgCl_2$
16 µl	0.5 M EGTA
3200 µl	50% glycerol solution
20 µl	20% Triton™X-100 solution (add at the end)
40 µl	100 mM PMSF
40 µl	100 mM PIC 3
½ pill	cOmplete™ ULTRA Tablets, Mini, EASYpack PIC1 (Sigma-Aldrich)
22 µl	ddH_2O

O+ Buffer (2 ml):

125 µl	1 M tris-HCl, pH 6.8
400 µl	50% glycerol solution
1.4 µl	5% 2-mercaptoethanol (add at the end, chemical hood)
460 µl	10% SDS solution
4 µl	0.5 M EGTA
4 µl	0.5 M EDTA
20 µl	100 mM PMSF
40 µl	100 mM PIC 3
1/3 pill	cOmplete™ ULTRA Tablets, Mini, EASYpack PIC1 (Sigma-Aldrich)
965,6 µl	ddH_2O

Modified reassembly buffer (2 ml):

400 µl	0.5 M MES
2 µl	1 M $MgSO_4$
4 µl	0.5 M EGTA
4 µl	1 M DTT
1200 µl	50% glycerol solution
10 µl	20% Triton™X-100 solution (add at the end)
20 µl	100 mM PMSF
20 µl	100 mM PIC 3
1/3 pill	cOmplete™ ULTRA Tablets, Mini, EASYpack PIC1 (Sigma-Aldrich)
340 µl	ddH_2O

5x Laemmli buffer:

400 mM	tris-HCl pH 6.8
500 mM	DTT
10%	SDS
0.1%	bromphenol-blue

The protocol of this assay is based on Valencia et al. (2013); all working steps were carried out at 37°C to prevent depolymerization. Brains and DRG

neurons were isolated from WT and P1c$^{-/-}$ mice and homogenized in 2 ml (brain) or 300 µl (DRG neurons) extraction buffer using a mechanical tissue homogenizer for brain samples and a 0,7x30 mm injection needle for DRG neurons. Lysates were centrifuged for 2 minutes at 9 000 x rpm to receive a fraction with intact MTs (SN1= total lysate). The first third from SN1 was kept as total lysate and was diluted 1:4 for brain lysates and 1:1 for DRG lysates with the O+ buffer. The rest of the SN1 lysate was centrifuged in a vacuum Optima TLX Ultracentrifuge (Beckmann) at 40 000 x rpm and 37°C for 20 minutes to obtain a MT containing pellet fraction and a MT free supernatant. The MT containing pellets were resuspended with the modified reassembly buffer. The pellet fraction and MT-free supernatant of brain sample were mixed with O+ buffer, for DRG sample only MT-free supernatant was mixed with O+ buffer. For detailed sample preparation see table 1 below. At last 5x Laemmli buffer was added and all samples were boiled for 5 min at 95°C.

Notes: 1. For DRG neurons use at least 5 mice to gain enough cells for lysis.

2. Isolation of DRG neurons should be as fast as possible, lasting not longer than 30 minutes for group of 5 mice. If necessary, mice should be processed individually, or in small groups (2 or 3), and should then be pooled after homogenization.

	SN1 lysate	**SN2 lysate**	**Pellet Fraction**
Brain	100 µl total lysate	80 µl SN2 lysate	SN2 Pellet + 100 µl Reassembly buffer
	400 µl O+ buffer	320 µl O+ buffer	400 µl O+ buffer
	125 µl 5x Laemmli buffer	100 µl 5x Laemmli buffer	125 µl 5x Laemmli buffer
	SN1 lysate	**SN2 lysate**	**Pellet Fraction**
DRG neurons	20 µl total lysate	50 µl SN2 lysate	SN2 Pellet + 40 µl Reassembly buffer
	20 µl O+ buffer	50 µl O+ buffer	
	10 µl 5x Laemmli buffer	25 µl 5x Laemmli buffer	10 µl 5x Laemmli buffer

Table 1 detailed list of sample preparation

SDS-Polyacrylamide gel electrophoresis (PAGE)

Buffers and solutions:

30% acrylamide-mix:

29 g	acrylamide
1 g	Bis-acrylamide
ddH_2O up to 100 ml	

SDS-page running buffer:

25 mM	tris-HCl pH 8.3
250 mM	glycine
0.1%	SDS

Proteins were separated using standard SDS- 10% PAGE (LAEMMLI 1970). Gels were prepared using the Mini-PROTEAN® Electrophoresis System (Bio-Rad). First, the cassette was filled with resolving gel, overlaid with isopropanol to polymerize. After removing the isopropanol the stacking gel was poured on top of the resolving gel, and a comb was inserted to allow slot formation for sample loading. Samples were boiled at 95°C for 5 min prior to loading into the gel slots. Gels were run at 25 mAmp/gel and 500 V.

Reagent	Resolving gel 10% (10 ml)	Stacking gel 5% (3 ml)
dH_2O	4 ml	2.1 ml
30% acrylamide mix	3.3 ml	0.5 ml
1.5 M tris-HCl, pH 8.8	2.5 ml	-
1 M tris-HCl pH 6.8	-	0.38 ml
10% SDS	0.1 ml	0.03 ml
10% ammonium persulfate	0.1 ml	0.03 ml
TEMED	0.004 ml	0.003

Table 2 preparation of SDS-PAGE gels

Immunoblotting and quantification

Buffers and solutions:

Ponceau S staining solution:

0.5% (w/v)	Ponceau S (Sigma-Aldrich)
1%	acetic acid
ddH_2O up to 1000 ml	

TBS buffer:

8.76 g	NaCl
2.42 g	tris-HCl pH 7.4
ddH_2O up to 1000 ml	

TBS-T buffer:

1000 ml	TBS buffer
1 ml	0.1% tween-20

Blot buffer:

48 mM	tris-HCl
40 mM	glycine
1%	SDS
pH 9.0	

Blocking solution:

25 g	BSA
450 ml	TBS-T buffer
50 ml	NaN_3

After electrophoresis, the separated proteins were transferred from the acrylamide-gels onto nitrocellulose membranes, via a Western-blot system, at 25 V and 500 mA, at 4°C, overnight; or 500 V and 300 mA, at 4C° for 3 h. Transfer efficiency was tested by staining the membrane with Ponceau S (Sigma-Aldrich) and washing shortly with ddH_2O to visualize the transferred bands. Further the

membrane was distained with 1x TBS-T buffer for 10 minutes. To block the membrane, 5% BSA in TBS-T buffer was added and incubated for 1 h. Then, the membrane was incubated with primary antibodies diluted in 5% BSA in TBS-T buffer at 4°C overnight, washed afterward 3 times for 10 min with TBS-T buffer, and incubated with secondary antibodies diluted in TBS-T buffer at room temperature for 1 h. After incubation and another washing step the proteins were detected. Detection was carried out using chemiluminescent substrate „SuperSignal West Pico“ (ThermoFisher) and the emission signal was measured with the Fusion FX Detection System (Vilber Lourmat). Protein bands were quantified using QuantiScan v1.5 software (Biosoft, Cambridge, UK).

Statistics

Statistical evaluation and data analysis were done using Microsoft Excel 2010. An unpaired, two-tailed Student´s t test (α= 0.05) or one-way analysis of variance (ANOVA; α= 0.05) was used comparing two groups or values of multiple groups. Tukey´s post-hoc test was used to determine the significance between values of individual groups and controls. P-values *<0.05, **<0,01, and ***<0.001. Routinely at least 3 independent experiments were performed and evaluated for statistics.

Antibodies, antisera and dyes

Primary antibody/serum/dyes	**Antibody type**	**Dilution**	**Source**
Acetylated tubulin, T6793, clone 6-11B-1	monoclonal, mouse	1:300 (IFM)	Sigma- Aldrich
Actin, A-2066	polyclonal, rabbit	1:100 (IFM)	Sigma-Aldrich
Actin, A4700, clone AC-40	monoclonal, mouse	1:200 (IFM)	Sigma-Aldrich
GAPDH, G9545	polyclonal, rabbit	1:10000 (IB)	Sigma-Aldrich
Integrin β1	rat	1:100 (IFM)	Abcam
Neurofilament, clone 2F11	monoclonal, mouse	1:50 (IFM) 1:250 (IB)	Dako

Neurofilament	monoclonal rabbit	1:50 (IFM)	Cell Signaling
Neurofilament 200kDa, clone RT97	monoclonal, rat	1:10 (IFM)	Wood et al.1981
Paxillin	monoclonal, mouse	1:100 (IFM)	BD Transduction Laboratories
Dye against actin	Phalloidin conjugated with Texas Red –X, T-7471	1:100 (IFM)	Molecular Probes
Plectin 1c (P1c)	polyclonal, rabbit	1:200 (IFM) 1:500 (IB)	Fuchs et al. 2009
Plectin 1f (P1f)	serum, rabbit	1:10 (IFM) 1:200 (IB)	Rezniczek et al. 2007
Plectin #46	serum, rabbit	1:100 (IFM)	Andrä et al. 2003
Talin	monoclonal, mouse	1:100 (IFM)	Sigma-Aldrich
Tau, A-0024	polyclonal, rabbit	1:200 (IFM) 1:10000 (IB)	Dako
Tau	mouse	1:200 (IFM)	Dako
α Tubulin, SM2202P, clone YL 1/2	monoclonal, rat	1:300 (IFM)	Acris antibodies
α Tubulin, T5168, clone B-5-1-2	monoclonal, mouse	1:1000 (IFM) 1:10000 (IB)	Sigma-Aldrich
Vimentin	polyclonal, goat	1:50 (IFM)	Giese and Traub 1986
Vinculin, clone Vin-11-5	monoclonal, mouse	1:50 (IFM)	Sigma-Aldrich

Table 3. Primary antibodies and serum used for immunoblotting (IB) and immunofluoresence microscopy (IFM) experiments

Secondary antibody	**Host**	**Dilution**	**Source**
Alexa Fluor 488 anti-mouse IgGs	goat	1:1000 (IFM)	Jackson ImmunoResearch Laboratories, Inc. (J.I.R)
Alexa Fluor 488 anti-rabbit IgGs	donkey	1:1000 (IFM)	J.I.R
AMCA anti-mouse	donkey	1:100 (IFM)	J.I.R
AMCA anti-rabbit	donkey	1:100 (IFM)	J.I.R
Cy5 anti-mouse IgGs	donkey	1:300 (IFM)	J.I.R
Cy5 anti-rabbit IgGs	donkey	1:300 (IFM)	J.I.R
Cy5 anti-rat IgGs	donkey	1:300 (IFM)	J.I.R

DyLight 649 anti-mouse IgGs	donkey	1:500 (IFM)	J.I.R
DyLight 649 anti-rabbit IgGs	donkey	1:500 (IFM)	J.I.R
DyLight 649 anti-rat IgGs	donkey	1:500 (IFM)	J.I.R
HRPO anti- mouse IgGs	goat	1:10000 (IB)	J.I.R
HRPO anti-rabbit IgGs	goat	1:20000 (IB)	J.I.R
HRPO anti-rat IgGs	goat	1:5000 (IB)	J.I.R
Rhodamine red anti-mouse IgGs	donkey	1:200 (IFM)	J.I.R
Rhodamine red anti-rabbit IgGs	donkey	1:200 (IFM)	J.I.R
Rhodamine red anti-rat IgGs	donkey	1:200 (IFM)	J.I.R
Texas red anti-mouse IgGs	donkey	1:200 (IFM)	J.I.R
Texas red anti-rabbit IgGs	donkey	1:200 (IFM)	J.I.R
Texas red anti-rat IgGs	goat	1:200 (IFM)	J.I.R

Table 4. Secondary antibodies used in IB and IFM experiments

Index for figures

Abbreviations

ABD	actin binding domain
ADP	adenosine diphosphate
ATP	adenosine triphosphate
BSA	bovine serum albumin
CNS	central nervous system
DMEM	Dulbecco´s modified eagle medium
DNA	deoxyribonucleic acid
DRG	dorsal root ganglia
DTT	dithiothreitol
EDTA	ethane (-1,2-diyldinitrilo) tetra-acetic acid
EGTA	ethylene glycol-bis (2-aminoethylether)
F-actin	filamentous actin
G-actin	globular actin
FRAP	fluorescence recovery after photobleaching
GAPDH	glyceraldehyde-3-phosphate dehydrogenase
GDP	guanosine-di-phosphate
GFP	green fluorescence protein
GTP	guanosine- tri- phosphate
HBSS	Hank´s Balanced Salt Solution
HEPES	4-(2-hydroxyethyl)-1-piperazineethanesulfonic acid
HMW	high molecular weight
HS	Horse serum
IF	intermediated filament
kDa	kilo dalton
KO	knock out
MAP	microtubule - associated protein
MES	2-(N-morpholino)ethane sulfonic acid
MF	microfilament
MT	microtubule
NF	neurofilament
P0	plectin full knock out
P1c	plectin isoform 1c

P1c$^{-/-}$	plectin 1c knock out
PBS	phosphate-buffered saline
PDL	poly-D-lysine
Pen/Strep	penicillin-streptomycin
PIC 1/3	phosphatase/ protease inhibitor cocktail
PLL	poly-L-lysine
PMSF	phenylmethylsulphonyl fluoride
PNS	peripheral nervous system
SDS	sodium dodecyl sulfate
SH3	Scr-homology 3 domain
TBS	tris-buffered saline
TBS-T	tris-buffered saline with 0,05% tween 20
TEMED	tetramethylethylene-1,2-diamine
WT	wild type

References

Akhmanova A, Steinmetz MO. 2008. Tracking the ends: A dynamic protein network controls the fate of microtubule tips. *Nature Reviews. Molecular Cell Biology* 9 (4): 309–22.

Andrä K, Kornacker I, Jörgl A, Zörer M, Spazierer D, Fuchs P, Fischer I, Wiche G. 2003. Plectin-isoform-specific rescue of hemidesmosomal defects in plectin (-/-) keratinocytes. *The Journal of Investigative Dermatology* 120 (2): 189–97.

Andrä K, Lassmann H, Bittner R, Shorny S, Fässler R, Propst F, Wiche G. 1997. Targeted inactivation of plectin reveals essential function in maintaining the integrity of skin, muscle, and heart cytoarchitecture. *Genes and Development* 11 (23): 3143–56.

Baas PW, Qiang L. 2019. Tau: It's not what you think. *Trends in Cell Biology* 29 (6): 452–61.

Baas PW, Rao AN, Matamoros AJ, Lanfranco L. 2016. Stability properties of neuronal microtubules. 73 (9): 442–60.

Banwell BL, Russel J, Fukudome T, Shen XM, Stilling G, Engel AG. 1999. Myopathy, myasthenic syndrome, and epidermolysis bullosa simplex due to plectin deficiency. *Journal of Neuropathology and Experimental Neurology* 58 (8): 832–46.

Breuzard G, Hubert P, Nouar R, De Bessa T, Devred F, Barbier P, Sturgis JN, Peyrot V. 2013. Molecular mechanisms of tau binding to microtubules and its role in microtubule dynamics in live cells. *Journal of Cell Science* 126 (13): 2810–19.

Brown A, Wang L, Jung P. 2005. Stochastic simulation of neurofilament transport in axons: the "Stop-and-Go" hypothesis. *Molecular Biology of the Cell* 16 (9): 4243–55.

Bulinski JC, Richards JE, Piperno G. 1988. Posttranslational modifications of alpha tubulin: detyrosination and acetylation aifferentiate populations of interphase microtubules in cultured cells. *Journal of Cell Biology* 106 (4): 1213–20.

Burgstaller G, Gregor M, Winter L, Wiche G. 2010. Keeping the vimentin network under control: cell-matrix adhesion-associated plectin 1f affects cell shape

and polarity of fibroblasts. *Molecular Biology of the Cell* 21 (19): 3362–75.

Cammarata GM, Bearce EA, Lowery LA. 2016. Cytoskeletal social networking in the Ggowth cone: how +TIPs mediate microtubule-actin cross-linking to drive axon outgrowth and guidance. *Cytoskeleton (Hoboken, N.J.)* 73 (9): 461–76.

Castañón MJ., Walko G, Winter L, Wiche G. 2013. Plectin-intermediate filament partnership in skin, skeletal muscle, and peripheral nerve. *Histochemistry and Cell Biology* 140 (1): 33–53.

Chapin SJ, Bulinski JC, Gundersen GG. 1991. Microtubule bundling in cells. *Nature* 349 (6304): 24.

Conde C, Cáceres A. 2009. Microtubule assembly, organization and dynamics in axons and dendrites. *Nature Reviews. Neuroscience* 10 (5): 319–32.

Couchie D, Mavilia C, Georgieff IS, Liem RK, Shelanski ML, Nunez J. 1992. Primary structure of high molecular weight tau present in the peripheral nervous system. *Proceedings of the National Academy of Sciences of the United States of America* 89 (10): 4378–81.

Craig AM, Banker G. 1994. Neuronal polarity. *Annual Review of Neuroscience* 17:1: 267–310.

Creppe C, Malinouskaya L, Volvert ML, Gillard M, Close P, Malaise O, Laguesse S, et al. 2009. Elongator controls the migration and differentiation of cortical neurons through acetylation of alpha-tubulin. *Cell* 136 (3): 551–64.

Dawson HN, Cantillana V, Jansen M, Wang H, Vitek MP, Wilcock DM, Lynch JR, Laskowitz DT. 2010. Loss of tau elicits axonal degeneration in a mouse model of Alzheimer's disease. *Neuroscience* 169 (1): 516–31.

Dehmelt L, Halpain S. 2004. The MAP2/tau family of microtubule-associated proteins. *Genome Biology* 6 (1): 204.

Dent EW, Gertler FB. 2003. Cytoskeletal dynamics and transport in growth cone motility and guidance. *Neuron* 40 (2): 209–27.

Dent EW, Gupton SL, Gertler FB. 2011. The growth cone cytoskeleton in axon outgrowth and guidance. *Cold Spring Harbor Perspectives in Biology 3(3)* 1–40.

Dickson DW, Kouri N, Murray ME, Josephs KA. 2011. Neuropathology of frontotemporal lobar degeneration-tau (FTLD-Tau). *Journal of Molecular Neuroscience : MN* 45 (3): 384–89.

Dixit R, Ross JL, Goldman YE, Holzbaur ELF. 2008. Differential regulation of

dynein and kinesin motor proteins by tau. *Science (New York, N.Y.)* 319 (5866): 1086–89.

Drechsel DN, Hyman AA, Cobb MH, Kirschner MW. 1992. Modulation of the dynamic instability of tubulin assembly by the microtubule-associated protein tau. *Molecular Biology of the Cell* 3 (10): 1141–54.

Elliott CE., Becker B, Oehler S, Castañón MJ, Hauptmann R, Wiche G. 1997. Plectin transcript diversity: identification and tissue distribution of variants with distinct first coding exons and rodless isoforms. *Genomics* 42 (1): 115–25.

England JD., Asbury AK. 2004. Peripheral neuropathy. *Lancet* 363 (9427): 2151–61.

Esmaeli-Azad B, McCarty JH, Feinstein SC. 1994. Sense and antisense transfection analysis of tau function: tau influences net microtubule assembly, neurite outgrowth and neuritic stability. *Journal of Cell Science* 107 (Pt 4 (April): 869–79.

Felgner H, Frank R, Biernat J, Mandelkow EM, Mandelkow E, Ludin B, Matus A, Schliwa M. 1997. Domains of neuronal microtubule-associated proteins and flexural rigidity of microtubules. *Journal of Cell Biology* 138 (5): 1067–75.

Fletcher DA, Dyche Mullins R. 2010. Cell mechanics and the cytoskeleton. *Nature* 463 (7280): 485–92.

Foisner R, Leichtfried FE, Herrmann H, Small JV, Lawson D, Wiche G. 1988. Cytoskeleton-associated plectin: in situ localization, in vitro reconstitution, and binding to immobilized intermediate filament proteins. *Journal of Cell Biology* 106 (3):723-733.

Foisner R, Wiche G. 1991. Intermediate filament-associated proteins. *Current Opinion in Cell Biology* 3 (1): 75–81.

Forrest K, Mellerio JE, Robb S, Dopping-Hepenstal PJC, McGrath JA, Liu L, Buk SJA, Al-Sarraj S, Wraige E, Jungbluth H. 2010. Congenital muscular dystrophy, myasthenic symptoms and epidermolysis bullosa simplex (EBS) associated with mutations in the PLEC1 gene encoding plectin. *Neuromuscular Disorders : NMD* 20 (11): 709–11.

Fuchs P, Zörer M, Reipert S, Rezniczek GA, FPropst F, Walko G, Fischer I et al. 2009. Targeted inactivation of a developmentally regulated neural plectin isoform (Plectin 1c) in mice leads to reduced motor nerve conduction velocity.

Journal of Biological Chemistry 284(39): 26502-26509

Fuchs P, Zörer M, Rezniczek GA, Spazierer D, Oehler S, Castañón MJ, Hauptmann R, Wiche G. 1999. Unusual 5′ transcript complexity of plectin isoforms: novel tissue-specific exons modulate actin binding activity. *Human Molecular Genetics* 8 (13): 2461–72.

Fukushima N, Furuta D, Hidaka Y, Moriyama R, a Tsujiuchi T. 2009. Post-translational modifications of tubulin in the nervous system. *Journal of Neurochemistry* 109 (3): 683–93.

Gache Y, Chavanas S, Lacour JP, Wiche G, Owaribe K, Meneguzzi G, Ortonne JP. 1996. Defective expression of plectin/HD1 in epidermolysis bullosa simplex with muscular dystrophy. *The Journal of Clinical Investigation* 97 (10): 2289–98.

Giese G, Traub P. 1986. Induction of vimentin synthesis in mouse myeloma cells MPC-11 by 12-0-tetradecanoylphorbol-13-acetate. *European Journal of Cell Biology* 40 (2): 266–74.

Glass JD, Griffin JW. 1994. Retrograde transport of radiolabeled cytoskeletal proteins in transected nerves. *The Journal of Neuroscience : The Official Journal of the Society for Neuroscience* 14 (6): 3915–21.

Goedert M, Jakes R. 1990. Expression of separate isoforms of human tau protein: correlation with the tau pattern in brain and effects on tubulin polymerization. *The EMBO Journal* 9 (13): 4225–30.

Goldberg DJ, Burmeister DW. 1986. Stages in axon formation: observations of growth of aplysia axons in culture using video-enhanced contrast-differential interference contrast microscopy. *Journal of Cell Biology* 103 (5): 1921–31.

Gregor M, Osmanagic-Myers S, Burgstaller G, Wolfram M, Fischer I, Walko G, Resch GP, Jörgl A, Herrmann H, Wiche G. 2014. Mechanosensing through focal adhesion-anchored intermediate filaments. *FASEB Journal* 28 (2): 715–29.

Gundersen GG 1989. Generation of a stable, posttranslationally modified microtubule array is an early event in myogenic differentiation. *The Journal of Cell Biology* 109 (5): 2275–88.

Gundesli H, Talim B, Korkusuz P, Balci-Hayta B, Cirak S, Akarsu NA, Topaloglu H, Dincer P. 2010. Mutation in exon 1f of PLEC, leading to disruption of plectin isoform 1f, causes autosomal-recessive limb-girdle muscular

dystrophy. *American Journal of Human Genetics* 87 (6): 834–41.

Hammond JW, Huang CF, Kaech S, Jacobson C, Banker G, Verhey KJ. 2010. Posttranslational modifications of tubulin and the polarized transport of kinesin-1 in neurons. *Molecular Biology of the Cell* 21 (4): 572–83.

Herrmann H, Wiche G. 1987. Plectin and IFAP-300K are homologous proteins binding to microtubule-associated proteins 1 and 2 and to the 240-kilodalton subunit of spectrin. *The Journal of Biological Chemistry* 262 (3): 1320–25.

Iqbal K, Liu F, Gong C-X, Grundke-Iqbal I. 2010. Tau in Alzheimer disease and related tauopathies. *Current Alzheimer Research* 7 (8): 656–64.

Janke C, Montagnac G. 2017. Causes and consequences of microtubule acetylation. *Current Biology* 27(23): 1287-1292.

Janning D, Igaev M, Sündermann F, Brühmann J, Beutel O, Heinisch JJ, Bakota L, Piehler J, Junge W, Brandt R. 2014. Single-molecule tracking of tau reveals fast kiss-and-hop interaction with microtubules in living neurons. *Molecular Biology of the Cell* 25 (22): 3541–51.

Jeanneteau F, KDeinhardt K, Miyoshi G, Bennett AM, Chao V. 2010. The MAP kinase phosphatase, MKP-1, regulates BDNF-induced axon branching 13 (11): 1373–79.

Kaneko T, Lei L, Shawn S-C L. 2008. The SH3 domain--a family of versatile peptide- and protein-recognition module. *Frontiers in Bioscience : A Journal and Virtual Library* 13 (May): 4938–52.

Konieczny P, Fuchs P, Reipert S, Kunz WS, Zeöld A, Fischer I, Paulin D, Schröder R, Wiche G. 2008. Myofiber integrity depends on desmin network targeting to Z-disks and costameres via distinct plectin isoforms. *Journal of Cell Biology* 181 (4): 667–81.

Kornack DR, Giger RJ. 2005. Probing microtubule +TIPs: regulation of axon branching. *Current Opinion in Neurobiology* 15 (1): 58–66.

Koss-Harnes D, Høyheim B, Anton-Lamprecht I, Gjesti A, Jørgensen RS, Jahnsen FL, Olaisen B, Wiche G, Gedde-Dahl T. 2002. A site-specific plectin mutation causes dominant epidermolysis bullosa simplex ogna: two identical de novo mutations. *The Journal of Investigative Dermatology* 118 (1): 87–93.

L'Hernault SW, Rosenbaum JL. 1985. Reversal of the posttranslational modification on chlamydomonas flagellar alpha-tubulin occurs during flagellar resorption. *The Journal of Cell Biology* 100 (2): 457–62.

LAEMMLI UK. 1970. Cleavage of structural proteins during the assembly of the head of bacteriophage T4'. *Nature* 227 (5259): 680–85.

Liu CG, Maercker C, Castañon MJ, Hauptmann R, Wiche G. 1996. Human plectin: organization of the gene, sequence analysis, and chromosome localization (8q24). *Proceedings of the National Academy of Sciences of the United States of America* 93 (9): 4278–83.

Mandelkow E, Mandelkow EM. 1995. Microtubules and microtubule-associated proteins. *Current Opinion in Cell Biology* 7 (1): 72–81.

Natsuga K, Nishie W, Akiyama M, Nakamura H, Shinkuma S, McMillan JR, Nagasaki A et al. 2010. Plectin expression patterns determine two distinct subtypes of epidermolysis bullosa simplex. *Human Mutation* 31 (3): 308–16.

Neve RL, Harris P, Kosik KS, Kurnit DM, Donlon TA. 1986. Identification of cDNA clones for the human microtubule-associated protein tau and chromosomal localization of the genes for tau and microtubule-associated protein 2. *Brain Research* 387 (3): 271–80.

Nunez J, Fischer I. 1997. Microtubule-associated proteins (MAPs) in the peripheral nervous system during development and regeneration. *Journal of Molecular Neuroscience : MN* 8 (3): 207–22.

Osmanagic-Myers S, Gregor M, Walko G, Burgstaller G, Reipert S, Wiche G. 2006. Plectin-controlled keratin cytoarchitecture affects MAP kinases involved in cellular stress response and migration. *Journal of Cell Biology* 174 (4): 557–68.

Perdiz D, Mackeh R, Poüs C, Baillet A. 2011. The ins and outs of tubulin acetylation: more than just a post-translational modification? *Cellular Signalling* 23 (5): 763–71.

Perez M, Santa-Maria I, Gomez De Barreda E, Zhu X, Cuadros R, Cabrero JR, Sanchez-Madrid F, et al. 2009. Tau - an inhibitor of deacetylase HDAC6 function. *Journal of Neurochemistry* 109 (6): 1756–66.

Piperno G, LeDizet M, Chang XJ. 1987. Microtubules containing acetylated alpha-tubulin in mammalian cells in culture. *The Journal of Cell Biology* 104 (2): 289–302.

Planel E, Krishnamurthy P, Miyasaka T, Liu L, Herman M, Kumar A, Bretteville A et al. 2008. Anesthesia-induced hyperphosphorylation detaches 3-repeat tau from microtubules without affecting their stability in vivo. *Journal of*

Neuroscience 28 (48): 12798-12807

Podgorny P, Toth C. 2014. Parkinson ’s disease and peripheral neuropathy. In Rana AQ, editor. A Synopsis of Parkinson´s Disease. IntechOpen p-101

Portran D, Schaedel L, Xu Z, Théry M, Nachury MV 2017. Tubulin acetylation protects long-lived microtubules against mechanical ageing. *Nature Cell Biology* 19 (4): 391–98.

Qiang L, Sun X, Austin TO, Muralidharan H, Jean DC, Liu M, Yu W, Baas PW. 2018. Tau does not stabilize axonal microtubules but rather enables them to have long labile domains. *Current Biology* 28 (13): 2181-2189

Qiang L, Yu W, Liu M, Solowska JM, Baas PW 2010. Basic fibroblast growth factor elicits formation of interstitial axonal branches via enhanced severing of microtubules. *Molecular Biology of the Cell* 21: 334–44.

Ranson SW, Clark SL. The Anatomy of the Nervous System. 10th ed. Philadelphia: WB Saunders Co, 1959:334 –335

Reipert S, Steinböck F, Fischer I, Bittner RE, Zeöld A, Wiche G. 1999. Association of mitochondria with plectin and desmin intermediate filaments in striated muscle. *Experimental Cell Research* 252 (2): 479–91.

Rezniczek GA, Abrahamsberg C, Fuchs P, Spazierer D, Wiche G. 2003. Plectin 5’-transcript diversity: short alternative sequences determine stability of gene products, initiation of translation and subcellular localization of isoforms. *Human Molecular Genetics* 12 (23): 3181–94.

Rezniczek GA, Walko G, Wiche G. 2010. Plectin gene defects lead to various forms of epidermolysis bullosa simplex. *Dermatologic Clinics* 28 (1): 33–41.

Samsonov A, Yu J-Z, Rasenick M, Popov SV. 2004. Tau interaction with microtubules in vivo. *Journal of Cell Science* 117 (Pt 25): 6129–41.

Schröder R, Schoser B. 2009. Myofibrillar myopathies: A clinical and myopathological guide. *Brain Pathology (Zurich, Switzerland)* 19 (3): 483–92.

Seibenhener ML, Wooten MW. 2012. Isolation and culture of hippocampal neurons from prenatal mice. *Journal of Visualized Experiments*, no.65: 4–9.

Sevcík J, Urbániková L, Kost’an J, Janda L, Wiche G. 2004. Actin-binding domain of mouse plectin. Crystal structure and binding to vimentin. *European Journal of Biochemistry* 271 (10): 1873–84.

Sghirlanzoni A, Pareyson D, Lauria G. 2005. Sensory neuron diseases. *The*

Lancet. Neurology 4 (6): 349–61.

Smith FJ, Eady RA, Leigh IM, McMillan JR, Rugg EL, Kelsell DP, Bryant SP et al. 1996. Plectin deficiency results in muscular dystrophy with epidermolysis bullosa. *Nature Genetics* 13 (4): 450–57.

Sokolowski K, Corbin JG. 2012. Wired for behaviors: From development to function of innate limbic system circuitry. *Frontiers in Molecular Neuroscience* 5 (April): 1–15.

Stamer K, Vogel R, Thies E, Mandelkow E, Mandelkow EM. 2002. Tau blocks traffic of organelles, neurofilaments, and APP vesicles in neurons and enhances oxidative stress. *Journal of Cell Biology* 156 (6): 1051–63.

Steinböck FA, Wiche G. 1999. Plectin: A cytolinker by design. *Biological Chemistry* 380 (2): 151–58.

Steinböck FA, Nikolic B, Coulombe PA, Fuchs E, Traub P, Wiche G. 2000. Dose-dependent linkage, assembly inhibition and disassembly of vimentin and cytokeratin 5/14 filaments through plectin's intermediate filament-binding domain. *Journal of Cell Science* 113 (Pt 3 (February): 483–91.

Stroissnigg H, Trančíková A, Descovich L, Fuhrmann J, Kutschera W, Kostan J, Meixner A, Nothias F, Propst F. 2007. S-nitrosylation of microtubule-associated protein 1B mediates nitric-oxide-induced axon retraction. *Nature Cell Biology* 9 (9): 1035–45.

Svitkina TM, Borisy GG. 1999. Arp2/3 complex and actin depolymerizing factor/cofilin in dendritic organization and treadmilling of actin filament array in lamellipodia. *The Journal of Cell Biology* 145 (5): 1009–26.

Tian R, Gregor M, Wiche G, Goldman JE. 2006. Plectin regulates the organization of glial fibrillary acidic protein in Alexander disease. *The American Journal of Pathology* 168 (3): 888–97.

Trinczek B, Biernat J, Baumann K, Mandelkow EM, Mandelkow E. 1995. Domains of tau protein, differential phosphorylation, and dynamic instability of microtubules. *Molecular Biology of the Cell* 6 (12): 1887–1902.

Uchida A, Brown A. 2004. Arrival, reversal, and departure of neurofilaments at the tips of growing axons. V'. *Molecular Biology of the Cell* 15: 4215–25.

Valencia RG, Mihailovska E, Winter L, Bauer K, Fischer I, Walko G, Jorgacevski J, Potokar M, Zorec R, Wiche G. 2020. Plectin dysfunction in neurons leads to tau accumulation on microtubules affecting neuritogenesis, organelle

trafficking, pain sensitivity and memory. *Neuropathology and Applied Neurobiology*, June, nan.12635.

Valencia R. 2012. Role of plectin in microtubule dynamics. Dissertation thesis at the University of Vienna

Valencia RG, Walko G, Janda L, Novacek J, Mihailovska E, Reipert S, Andrä-Marobela K, Wiche G. 2013. Intermediate filament-associated cytolinker plectin 1c destabilizes microtubules in keratinocytes.

Verhey KJ, Gaertig J. 2007. The tubulin code. *Cell Cycle (Georgetown, Tex.)* 6 (17): 2152–60.

Wang L, Brown A. 2001. Rapid intermittent movement of axonal neurofilaments observed by fluorescence photobleaching. *Molecular Biology of the Cell* 12 (10): 3257–67.

Watson DF, Glass JD, Griffin JW. 1993. Redistribution of cytoskeletal proteins in mammalian axons disconnected from their cell bodies. *The Journal of Neuroscience : The Official Journal of the Society for Neuroscience* 13 (10): 4354–60.

Weingarten MD, Lockwood AH, Hwo SY, Kirschner MW. 1975. A protein factor essential for microtubule assembly. *Proceedings of the National Academy of Sciences of the United States of America* 72 (5): 1858–62.

Westermann S, Weber K 2003. Post-translational modifications regulate microtubule function. *Nature Reviews Molecular Cell Biology 4*, 938–48.

Wiche G, Becker B, Luber K, Weitzer G, Castañòn MJ, Hauptmann R, Stratowa C, Stewart M. 1991. Cloning and sequencing of rat plectin indicates a 466-kD polypeptide chain with a three-domain structure based on a central alpha-helical coiled coil. *The Journal of Cell Biology* 114 (1): 83–99.

Wiche G, Baker MA. 1982. Cytoplasmic network arrays demonstrated by immunolocalization using antibodies to a high molecular weight protein present in cytoskeletal preparations from cultured cells. *Experimental Cell Research* 138 (1): 15–29.

Wiche G, Osmanagic-myers S, Castañòn MJ. 2015. Networking and anchoring through plectin : A key to IF functionality and mechanotransduction. Curr Opin Cell Biology 2015 (Feb), 32:21-9

Wiche G, Winter L. 2011. Plectin isoforms as organizers of intermediate filament cytoarchitecture. *Bioarchitecture* 1 (1): 14–20.

Williams DR. 2006. Tauopathies: classification and clinical update on neurodegenerative diseases associated with microtubule-associated protein tau. *Internal Medicine Journal* 36 (10): 652–60.

Wilson PJ, Forer A. 1997. Effects of nanomolar taxol on crane-fly spermatocyte spindles indicate that acetylation of kinetochore microtubules can be used as a marker of poleward tubulin flux. *Cell Motility and the Cytoskeleton* 37 (1): 20–32.

Winter L, Wiche G. 2013. The Many Faces of Plectin and Plectinopathies: Pathology and Mechanisms'. *Acta Neuropathologica* 125 (1):77-93

Witte H, Neukirchen D, Bradke F. 2008. Microtubule stabilization specifies initial neuronal polarization. *Journal of Cell Biology* 180 (3): 619–32.

Wood JN, Anderton BH. 1981. Monoclonal antibodies to mammalian neurofilaments. *Bioscience Reports* 1 (3): 263–68.

Yu W, Qiang L, Solowska JM, Karabay A, Korulu S, Baas PW. 2008. The microtubule-severing proteins spastin and katanin participate differently in the formation of axonal branches. *Molecular Biology of the Cell* 19: 1485–98.

Yuan A, Kumar A, Peterhoff C, Duff K, Nixon RA. 2008. Axonal transport rates in vivo are unaffected by tau deletion or overexpression in mice. *The Journal of Neuroscience : The Official Journal of the Society for Neuroscience* 28 (7): 1682–87.

Zeitelhofer M, Vessey JP, Yunli Xie Y, Tübing F, Thomas S, Kiebler M, Dahm R. 2007. High-efficiency transfection of mammalian neurons via nucleofection. *Nature Protocols*. 2(7):1692-704